Version of Record: https://www.sciencedirect.com/science/article/pii/S2451904922000713
Manuscript_95dcf0b83ec3b53c484c7d21c350ad55

Convective heat transfer and friction factor characteristics of molten salts in spirally fluted tubes

Sheng Zhang* and Xiaodong Sun*

Department of Nuclear Engineering and Radiological Sciences, University of Michigan, Ann Arbor, MI 48109, United States

ABSTRACT

Spirally fluted tubes have been widely used for heat exchangers due to their superior heat transfer enhancement. However, most of the previous studies focused on the effects of a limited number of geometric parameters, i.e., the flute pitch and flute depth, on convective heat transfer and friction factor characteristics of low-Prandtl-number fluids, i.e., air or water. The correlations developed in these studies may not be accurate or applicable for medium-Prandtl-number fluids, such as molten salts. A numerical analysis using a Computational Fluid Dynamics (CFD) tool, STAR CCM+, is therefore carried out in this study to systematically investigate the effects of four geometric parameters, including the flute pitch p, flute depth e, flute start number N_s (or flute helix angle θ), and trough length L_{tr} on convective heat transfer and friction factor characteristics of a medium-Prandtl-number fluid, FLiNaK (46.5LiF-11.5NaF-42KF mol %), in spirally fluted tubes. In addition, the convective heat transfer and Darcy friction factor correlations are proposed and validated, with ±20% uncertainties, for medium-Prandtl-number fluids under the following conditions: Re = 88 to 1,600, Pr = 2.5 to 40, $p/D_c = 0.44$ to 3.51, $e/D_c = 0.10$ to 0.40, $\theta/90 = 0.20$ to 0.81, and $L_{tr}/D_c = 0.71$ to 2.16. The correlations proposed help improve the design of spirally fluted-tube heat exchangers.

KEYWORDS

Spirally fluted tube; Convective heat transfer; Friction factor; Molten salt; Laminar flow.

Nomenclature

A_h	equivalent heat transfer area, m^2
c_p	fluid specific heat capacity, J/kg-K
D_{A_f}	cross-sectional area based diameter, m
D_{bi}	inner bore diameter, m

*: Corresponding author at: University of Michigan, 2355 Bonisteel Blvd., Ann Arbor, MI 48109-2104, USA.
E-mail address:shengzh@umich.edu, xdsun@umich.edu

D_{bo} outside bore diameter, m

D_c characteristic length (or equivalent diameter), m

D_{eo} outside envelop diameter, m

D_i inner diameter, m

e flute depth, m

e^* non-dimensional flute depth

f Darcy friction factor

$\bar{h}$ average heat transfer coefficient, W/m^2-K

k fluid thermal conductivity, W/m-K

L tube length, m

L_{tr} trough length, m

L_{tr}^* non-dimensional trough length

$\dot{m}$ mass flow rate, kg/s

$\dot{m}_t$ total mass flow rate, kg/s

N number of the spirally fluted tubes

N_s flute start number

Nu Nusselt number

p flute pitch, m

p^* non-dimensional flute pitch

Δp pressure drop, Pa

Δp_h pressure drop in the two headers of a tube bundle, Pa

Δp_t total pressure drop in a tube bundle (including the two headers) , Pa

Pr Prandtl number

$\dot{Q}$ heat transfer rate, W

Re Reynolds number

$\overline{T_f}$ arithmetic mean of the fluid bulk inlet and outlet temperatures , °C

$\overline{T_{in}}$ fluid bulk inlet temperature, °C

$\overline{T_{out}}$ fluid bulk outlet temperature, °C

$\overline{T_w}$ wall-surface-area-averaged temperature, °C

u fluid velocity, m/s

Greek symbols

δ	wall thickness, m
ψ_p	predicted value of a parameter ψ
ψ_t	true value of a parameter ψ
μ	fluid dynamic viscosity, kg/m-s
ρ	fluid density, kg/m^3
θ	flute helix angle, °
θ^*	non-dimensional flute helix angle

Abbreviations

CFD	computational fluid dynamics
GCI	grid convergence index
HX	heat exchanger
MSR	molten salt reactor
TB	tube bundle

1. Introduction

Various techniques on heat transfer enhancement are used in the design of heat exchangers (HXs), which are generally classified into two categories, (1) active method which needs external power, i.e., the surface vibration and (2) passive method without additional power, i.e., spirally fluted surface, coiled wire, and twisted-tape insert. These techniques increase heat transfer by reducing the thickness of the laminar sublayer or viscous layer, where thermal conduction, a heat transfer mechanism inferior to thermal convection, dominates heat transfer through the stagnant layer.

One promising passive technique on heat transfer enhancement is to adopt a spirally fluted tube that increases local turbulence on both the inner and outer surfaces of the tube. In addition, the spirally fluted tube usually has a much larger heat transfer area compared with a smooth tube for the same cross-sectional area (flow area). Due to enhanced heat transfer performance and large surface area, spirally fluted tubes have been proposed for the design of HXs in the Advanced High-Temperature Reactor [1] and the design of double-wall HXs to control tritium

leakage in the Fluoride-salt-cooled High-temperature Reactor [2]. In addition, they have been widely used for low-temperature applications, i.e., residential heating and air-conditioning [3].

There are a number of publications focused on spirally fluted tubes as summarized in Table 1. Srinivasan et al. [4-6] experimentally investigated heat transfer and friction factor for water in spirally fluted tubes for different flute pitches p, flute depths e, flute helix angles θ, Reynolds numbers Re, and Prandtl numbers Pr , while Garimella and Christensen [7-8] experimentally investigated thermal-hydraulic performance of water flowing in different annuli, where the smooth tubes and spirally fluted tubes were used as the inner and outer tubes, respectively. In their studies [4-6], the heat transfer enhancement ratio, defined as the ratio of the Nusselt number between the spirally fluted tube and smooth tube $\mathrm{Nu}_f/\mathrm{Nu}_s$, was up to 10.0 for laminar flows and 2.6 for turbulent flows. As for the friction factor ratio, defined as the ratio of the friction factor between the spirally fluted tube and smooth tube f_f/f_s, was up to 2.0 for laminar flows and 10.0 for turbulent flows.

Table 1 Previous studies on spirally fluted tubes

Exp. or CFD study	Fluid	Tube dimensions	Characteristic length (D_c)	Enhancement	Ref.
Exp.	Ethylene-glycol solution and water (tube side)	N_s = 3; e/D_c = 0.125; p/D_c = 1.020; $\theta/90$ = 0.556; D_c = 12.75 mm;	Inner diameter of the smooth section	Nu_f / Nu_s > 8; f_f / f_s < 3	[3]
Exp.	Water (tube side)	N_s = 1 to 5; e/D_c = 0.11 to 0.42; p/D_c = 0.41 to 7.29; $\theta/90$ = 0.28 to 0.65; D_c = 8.79 to 18.97 mm;	Inside volumetric diameter	Nu_f / Nu_s = 1.1 to 10.0; f_f / f_s = 1.1 to 10.0	[5]
Exp.	Water (shell side)	N_s = 1 to 5; e/D_c = 0.104 to 0.384; p/D_c = 0.383 to 6.714; $\theta/90$ = 0.279 to 0.652;	Hydraulic diameter	Nu_f / Nu_s = 4 to 20	[7]
Exp.	Water (shell side)	N_s = 3 to 5; e/D_c = 0.124 to 0.309; p/D_c = 0.358 to 1.302; $\theta/90$ = 0.431 to 0.671;	Hydraulic diameter	f_f / f_s = 1.1 to 2.0 for laminar flows and up to 10 for turbulent flows	[8]
Exp.	Ethylene-glycol	N_s = 1 e/D_c = 0.02 to 0.06;	Inside envelop diameter	Nu_f / Nu_s = 1.3 to 4.0; f_f / f_s = 1.2 to 4.0	[9]

	solution and water (tube side)	p/D_c = 0.6 to 1.2; D_c = 18 mm;			
Exp.	Ethoquad T13-50 and SPE98330 (tube side)	N_s = 4; D_c = 10.3 mm;	Inner diameter of the smooth section	$Nu_f / Nu_s > 1.2$; f_f / f_s = 2.6 to 3.5	[10]
Exp.	Water (tube side)	N_s = 4; e/D_c = 0.116 to 0.118; p/D_c = 0.450 to 0.525; D_c = 18.85 to 18.90 mm;	Inner diameter of the smooth section	$Nu_f / Nu_s < 2.72$; $f_f / f_s > 5$	[11]
Exp. and CFD	Water (tube side)	N_s = 3; e/D_c =0.18; p/D_c = 0.91 to 3.64; D_c = 11 mm;	Arithmetic average of the inside bore diameter and inside envelope diameter	Nu_f / Nu_s = 2.4 to 3.7; f_f / f_s = 1.7 to 2.3	[12]
Exp.	Air (tube side)	N_s = 1 and 3; e/D_c = 0.02 to 0.056; p/D_c = 0.27 to 1.53; $\theta/90$ = 0.102 to 0.411; D_c = 23 mm	Inner diameter of the smooth section	$Nu_f / Nu_s < 2.15$; $f_f / f_s < 3.7$	[13]
CFD study	Water (shell side)	N_s = 1 to 4; e = 3 mm;	Hydraulic diameter	Nu_f / Nu_s = 1.05 to 1.10; f_f / f_s = 1.08 to 1.21	[14]
CFD study	Water (tube side)	N_s = 6; e/D_c = 0.09 to 0.28; p/D_c = 4.07 to 5.52; D_c = 8.0 to 12.3 mm	Inside envelope diameter	Nu_f / Nu_s = 1.1 to 1.3; f_f / f_s = 1.5 to 2.4	[15]
CFD study	Water (tube side)	N_s = 6; e/D_c = 0.15 to 0.46; p/D_c = 0.77 to 2.31; D_c = 13 mm;	Arithmetic average of the inside bore diameter and inside envelope diameter	Nu_f / Nu_s = 2.4 to 3.7; f_f / f_s = 1.7 to 2.3	[16]
CFD study	Air (tube side)	N_s = 5; e/D_c = 0.06; p/D_c = 1.0 to 3.5; D_c = 50 mm	Inside envelope diameter	$Nu_f / Nu_s < 2.02$; $f_f / f_s < 6.12$	[17]
CFD study	Air (tube side)	N_s = 2 to 5; e/D_c = 0.02 to 0.16; p/D_c = 1.5; D_c = 50 mm	Inside envelope diameter	Nu_f / Nu_s = 0.8 to 2.2; f_f / f_s = 1.0 to 8.3	[18]

The large values of the heat transfer enhancement ratio and friction factor ratio were also identified in other experimental studies, as summarized in Table1, using ethylene-glycol solutions [3, 9], reducing surfactant solutions [10], water [11-12], and air [13] as the working

fluids. In addition, several numerical studies [14-18], as summarized in Table 1, focused on the effects of a limited number of geometric parameters on heat transfer and friction factor characteristics of low-Prandtl-number fluids in spirally fluted tubes. The identified findings may not be accurate or applicable for medium-Prandtl-number fluids, i.e., molten salts. It is therefore necessary to systematically investigate the effects of all key geometric parameters on heat transfer and friction factor characteristics of medium-Prandtl-number fluids in spirally fluted tubes.

A numerical study using a Computational Fluid Dynamics (CFD) tool, STAR CCM+, is carried out to investigate the effects of the flute pitch p, flute depth e, flute start number N_s (affecting the flute helix angle θ), and trough length L_{tr} on convective heat transfer and friction factor characteristics of a molten salt FLiNaK (46.5LiF-11.5NaF-42KF mol %) and water (as a reference) in spirally fluted tubes. In addition, new convective heat transfer and friction factor correlations are proposed for laminar flows in spirally fluted tubes and validated by comparing with the experiments using air (this study), water, and ethylene-glycol solution as the working fluids.

2. Numerical modeling

2.1.Geometric parameters

A spirally fluted tube is normally fabricated by twisting a smooth tube. The smooth tube has three geometric parameters, tube inner diameter D_i, wall thickness δ, and tube length L, while the spirally fluted tube, taking a three-start spirally fluted tube as an example as shown in Fig. 1, has seven basic geometric parameters, including the inner bore diameter D_{bi}, outside envelope diameter D_{eo}, wall thickness δ, flute pitch p, trough length L_{tr}, number of flute starts N_s, and tube length L (not shown in Fig. 1). The inner bore diameter is the maximum outer diameter of a smooth tube which can slip in the spirally fluted tube, while the outside envelope diameter is the minimum inner diameter of a smooth tube in which the spirally fluted tube can slip.

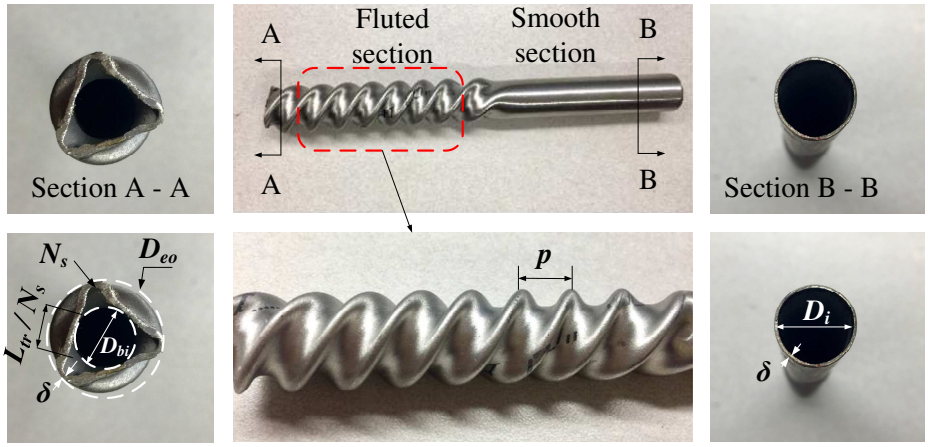

Fig. 1 A three-start spirally fluted tube

There are four non-dimensional geometric parameters widely used to characterize thermal-hydraulic performance of fluids in spirally fluted tubes, namely, the non-dimensional flute pitch p^*, non-dimensional flute depth e^*, non-dimensional trough length L_{tr}^*, and non-dimensional flute helix angle θ^* defined in Eqs. (1) to (4), respectively.

$$p^* = \frac{p}{D_c} \tag{1}$$

$$e^* = \frac{e}{D_c} \tag{2}$$

$$L_{tr}^* = \frac{L_{tr}}{D_c} \tag{3}$$

$$\theta^* = \frac{\theta}{90} \tag{4}$$

D_c is the characteristic length (or equivalent diameter) used to calculate the Reynolds number. A cross-sectional area A_f based diameter, defined as

$$D_{A_f} = \sqrt{\frac{4A_f}{\pi}} \tag{5}$$

is used as the characteristic length D_c for data reduction in this study.

Previous studies, as summarized in Table 1, defined the characteristic length of a spirally fluted tube in different ways, i.e., the inside volumetric diameter, hydraulic diameter, inside envelop diameter, inner diameter of the smooth section, and arithmetic average of the inside bore and inside envelop diameter. To have a meaningful comparison between the CFD results in this

study and experimental data in the literature, the experimental data are reprocessed if needed based on the characteristic length defined in Eq. (5).

The flute depth e is defined as

$$e = \frac{D_{eo} - D_{bo}}{2} \tag{6}$$

where the outside bore diameter D_{bo} is calculated by

$$D_{bo} = D_{bi} + 2\delta \tag{7}$$

The flute helix angle θ is defined as

$$\theta = \arctan\left[\frac{\pi(D_c + 2\delta)}{N_s p}\right] \tag{8}$$

Convective heat transfer and friction factor characteristics of FLiNaK (46.5LiF-11.5NaF-42KF mol %) and/or water in nineteen spirally fluted tubes, T#1 to T#19 as summarized in Table 2, are investigated in this study. The non-dimensional geometric parameters for these tubes are summarized in Table 3, where p^* = 0.44 to 3.51, e^* = 0.10 to 0.40, L_{tr}^* = 0.71 to 2.16, and θ^* = 0.20 to 0.81. In addition, new convective heat transfer and friction factor correlations are proposed and validated by comparing with the experiments, as summarized in Tables 2 and 3, using the spirally fluted tubes E#1 to E#4 as the test sections.

Table 2 Geometric parameters for sprially fluted tubes

Tube #	Working fluids	Measured parameters						Calculated parameter	Ref.
		D_{bi} (mm)	D_{eo} (mm)	δ (mm)	p (mm)	L_{tr} (mm)	N_s	D_c (mm)	
Numerical study (L = 762 mm)									
T#1	FLiNaK	10.11	17.15	0.51	5.49	22.30	3	12.50	This study
T#2	FLiNaK and water	10.11	17.15	0.51	11.73	22.30	3	12.50	
T#3	FLiNaK	10.11	17.15	0.51	21.94	22.30	3	12.50	
T#4	FLiNaK and water	10.11	17.15	0.51	32.91	22.30	3	12.50	
T#5	FLiNaK	10.11	17.15	0.51	43.88	22.30	3	12.50	
T#6	FLiNaK	10.11	13.22	0.51	11.73	22.30	3	10.34	
T#7	FLiNaK and water	10.11	15.51	0.51	11.73	22.30	3	12.16	
T#8	FLiNaK and water	10.11	19.90	0.51	11.73	22.30	3	13.14	

T#9	FLiNaK	10.11	22.10	0.51	11.73	22.30	3	13.75	
T#10	FLiNaK	10.11	17.15	0.51	11.73	22.30	1	11.10	
T#11	FLiNaK	10.11	17.15	0.51	11.73	22.30	2	11.10	
T#12	FLiNaK	10.11	17.15	0.51	11.73	22.30	4	12.16	
T#13	FLiNaK	10.11	17.15	0.51	11.73	22.30	5	11.82	
T#14	FLiNaK	10.11	17.15	0.51	11.73	22.30	6	11.47	
T#15	FLiNaK and water	10.11	17.15	0.51	11.73	9.52	3	13.45	
T#16	FLiNaK	10.11	17.15	0.51	11.73	12.70	3	13.14	
T#17	FLiNaK and water	10.11	17.15	0.51	11.73	15.87	3	12.82	
T#18	FLiNaK	10.11	17.15	0.51	11.73	19.05	3	12.82	
T#19	FLiNaK	10.11	17.15	0.51	11.73	25.40	3	12.50	
Experimental study									
E#1	Air	10.76[a]	18.37[a]	0.71[a]	10.00[a]	21.46[a]	3	12.97	This study
E#2	Water	10.11	17.15	0.51	11.73	22.30	3	12.50[b]	[5]
E#3	Water	10.21	18.80	0.51	13.26	19.68	3	12.82[b]	[5]
E#4	Ethylene-glycol solution	10.64[c]	15.88[c]	1.02	13	22.49[c]	3	12.75[c]	[3]

Notes:
a: An average value of the measurements at three locations/sections equally spaced was used for each geometric parameter with an associated uncertainty less than 1.4%;
b: Estimated values from 3D models constructed based on information in the literature [5];
c: Estimated values from an image in the literature [3].

Table 3 Non-dimensional geometric parameters for sprially fluted tubes

Tube #	p^*	e^*	L_{tr}^*	θ^*	References
Numerical study					
T#1	0.44	0.24	1.78	0.76	This study
T#2	0.94	0.24	1.78	0.56	
T#3	1.76	0.24	1.78	0.36	
T#4	2.63	0.24	1.78	0.26	
T#5	3.51	0.24	1.78	0.20	
T#6	1.13	0.10	2.16	0.50	
T#7	0.96	0.18	1.83	0.55	
T#8	0.89	0.33	1.70	0.57	
T#9	0.85	0.40	1.62	0.59	
T#10	1.06	0.27	2.01	0.81	
T#11	1.06	0.27	2.01	0.65	
T#12	0.96	0.25	1.83	0.46	
T#13	0.99	0.25	1.89	0.38	
T#14	1.02	0.26	1.94	0.32	

T#15	0.87	0.22	0.71	0.58	
T#16	0.89	0.23	0.97	0.57	
T#17	0.91	0.23	1.24	0.57	
T#18	0.91	0.23	1.49	0.57	
T#19	0.94	0.24	2.03	0.56	
Experimental study					
E#1	0.77	0.24	1.65	0.63	This study
E#2	0.94	0.24	1.78	0.56	[5]
E#3	1.03	0.30	1.54	0.53	[5]
E#4	1.02	0.13	1.76	0.56	[3]

2.2.Boundary conditions

The fluid domain in each of the nineteen spirally fluted tubes is constructed in STAR CCM+. Boundary conditions include a uniform mass flow rate inlet at 500 °C for FLiNaK and 20 °C for water in laminar flow regime (Re = 88 to 1,600), an atmospheric pressure outlet, and a constant wall heat flux of 20 kW/m^2 for FLiNaK and 1.5 kW/m^2 for water to study thermal performance (Nusselt number) or isothermal wall condition to study hydrodynamic performance (Darcy friction factor) of laminar flows in spirally fluted tubes.

Several mesh models, i.e., the polyhedral mesher, surface remesher, and prism layer mesher are enabled for meshing. The key physical models include laminar, liquid, polynomial density, segregated flow, segregated fluid enthalpy, and steady. In addition, the thermophysical properties of the FLiNaK salt recommended in the literature [19] are used in this study. It should be noted that the radiative heat transfer in the FLiNaK salt is neglected in this study, because the enhanced convection is the dominated form of heat transfer under conditions investigated, while it needs to be evaluated for molten salts in the reactor core of a Molten Salt Reactor (MSR) for high-accuracy predictions of reactor performance [19-20].

2.3.Data reduction for CFD results

2.3.1. Tube-side friction factor

The Darcy friction factor, defined as

$$f = \frac{2\rho D_c A_f^2}{L\dot{m}^2}\Delta p \tag{9}$$

is used to estimate the pressure loss, where $\dot{m}$, ρ, and Δp are the mass flow rate, fluid density, and pressure drop, respectively. It should be noted that Δp includes pressure drops due to frictional and form losses.

2.3.2. Tube-side Nusselt number

The tube-side Nusselt number is defined as

$$\mathrm{Nu} = \frac{\bar{h} D_c}{k} \tag{10}$$

where $\bar{h}$ and k are the average heat transfer coefficient and fluid thermal conductivity, respectively.

The average heat transfer coefficient is defined as

$$\bar{h} = \frac{\dot{Q}}{A_h(\bar{T}_w - \bar{T}_f)} \tag{11}$$

where $\dot{Q}$, A_h, $\bar{T}_w$, and $\bar{T}_f$ are the heat transfer rate, equivalent heat transfer area defined by Eq. (12), wall-surface-area-averaged temperature defined by Eq. (13), and arithmetic mean of the fluid bulk inlet and outlet temperatures defined by Eq. (14), respectively.

$$A_h = \pi D_c L \tag{12}$$

$$\bar{T}_w = \frac{\int T_w \mathrm{d}A}{A_w} \tag{13}$$

$$\bar{T}_f = \frac{1}{2}(\bar{T}_{in} + \bar{T}_{out}) \tag{14}$$

The fluid bulk inlet (or outlet) temperature is defined as

$$\bar{T}_{in} = \frac{\int \rho c_p u T_{in} \mathrm{d}A}{\int \rho c_p u \mathrm{d}A} \tag{15}$$

where u and c_p are the fluid velocity in the axial direction and fluid specific heat capacity, respectively.

In addition, the fluid Reynolds number and Prandtl number are calculated respectively as

$$\mathrm{Re} = \frac{\dot{m} D_c}{\mu A_f} \tag{16}$$

$$\mathrm{Pr} = \frac{\mu c_p}{k} \tag{17}$$

2.4.Grid independence study

The Grid Convergence Index (GCI) [21] has been widely used for the grid independence study. It is therefore adopted to investigate the spatial convergence of numerical results in this study. Taking FLiNaK in the spirally fluted tube T#2 as an example, three mesh options, as summarized in Table 4, are used for the grid independence study. The GCI values of the Nusselt number Nu and Darcy friction factor *f* are 1.32% and 1.71%, respectively. The CFD results using the fine mesh, as shown in Fig. 2, are therefore considered to be mesh independent, which are adopted in this study for thermal-hydraulic analysis of FLiNaK and/or water in spirally fluted tubes.

Table 4 Grid independence study for FLiNaK in the spirally fluted tube T#2 (Re = 1,600)

Mesh option	Cell quantity (10^6)	Grid size (mm)	Nu	*f*
1 (Fine)	3.753	0.292	58.040	0.157
2 (Medium)	1.655	0.384	59.314	0.163
3 (Coarse)	0.745	0.501	55.486	0.141
GCI (%)	N/A	N/A	1.32	1.71

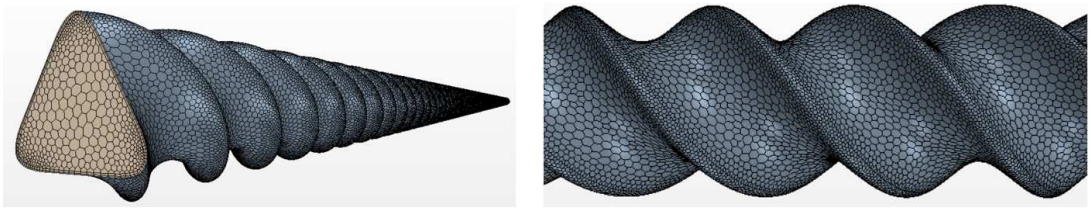

Fig. 2 Fine mesh for the fluid domain in T#2 (transverse and longitudinal cross-sections)

3. Experiments

Before applying the CFD tool STAR CCM+ for thermal-hydraulic analysis of FLiNaK and/or water in spirally fluted tubes, it is necessary to validate the numerical model initially by comparing with the experiments.

3.1.Tube-side friction factor

3.1.1. Shell-and-fluted-tube HXs

The tube-side Darcy friction factor for air flowing in two shell-and-fluted-tube HXs, as shown in Fig. 3, was investigated under isothermal conditions in this study. The Tube Bundles #1 and #2 (TB#1 and TB#2) of the two HXs were composed of eleven spirally fluted tubes (E#1) in a triangular configuration and twelve such tubes in an inline configuration, respectively.

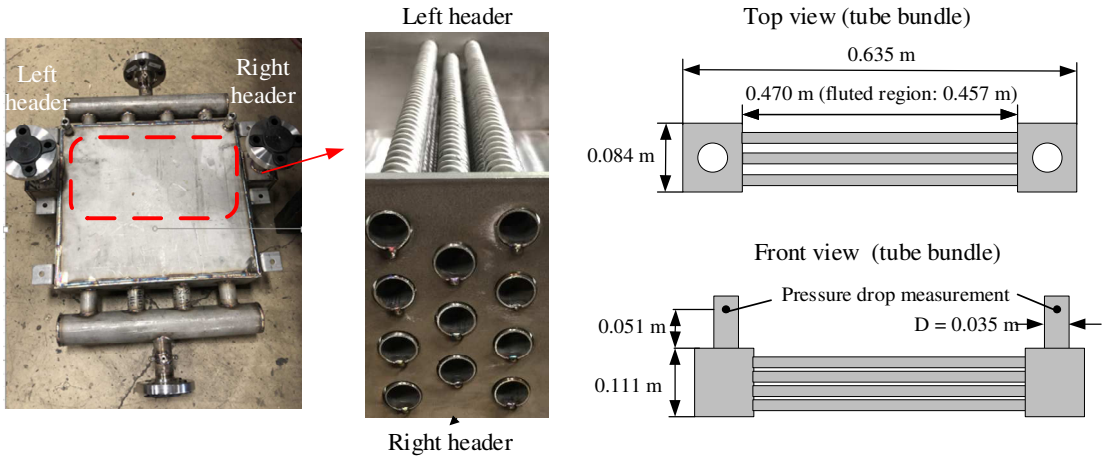

(a)

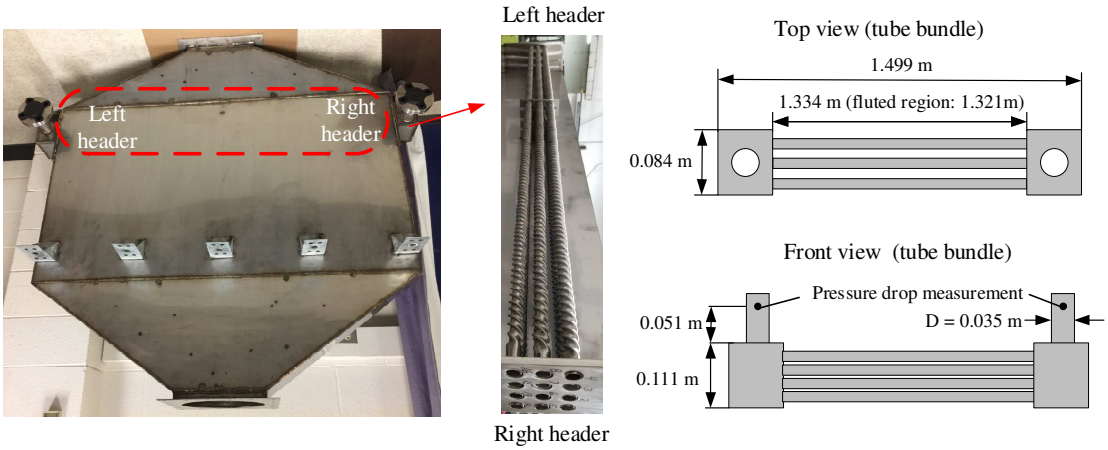

(b)

Fig. 3 Dimensions of (a) TB#1 and (2) TB#2

The flow rate was measured by a flow meter FMA1743A from Omega Engineering, Inc., providing a range of 0 - 200 L/min and accuracy of ±1.5% of the full scale. The differential pressure was measured by a differential pressure transducer STD800 from Honeywell Process,

Inc., with a span of 80 Pa and accuracy of ±0.32% of the span. The temperature was measured by a T type thermocouple with an accuracy of ±1.0 °C.

3.1.2. Uncertainty analysis

To calculate the Darcy friction factor, Eq. (9) is rewritten as follows,

$$f = \frac{4\rho A_f^{5/2}}{\sqrt{\pi} L (\dot{m}_t/N)^2} (\Delta p_t - \Delta p_h) \tag{18}$$

where Δp_t, Δp_h, $\dot{m}_t$, and N are the total pressure drop in a tube bundle (including the two headers), pressure drop in the two headers of the tube bundle, total mass flow rate, and number of the spirally fluted tubes.

Δp_h is predicted through a CFD study, while other parameters in Eq. (18) could be either measured or calculated. Fig. 4 shows the relationship between the flow rate and pressure drop. The pressure drop in one spirally fluted tube is obtained by subtracting the pressure drop in the two headers from the total pressure drop in the tube bundle.

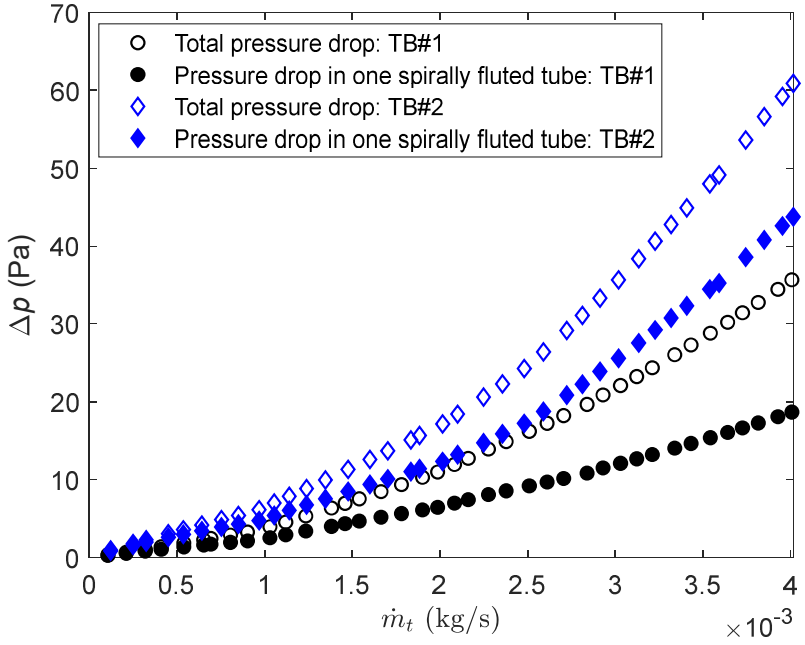

Fig. 4 Mass flow rate and pressure drop for air in the experiments

The uncertainty in the Darcy friction factor is estimated by an error propagation analysis as follows,

$$\frac{\sigma_f}{f} = \sqrt{\left(\frac{\sigma_\rho}{\rho}\right)^2 + \left(\frac{5}{2}\frac{\sigma_{A_f}}{A_f}\right)^2 + \left[\frac{\sigma_{\Delta p_t}}{\Delta p_t}\right]^2 + \left[\frac{\sigma_{\Delta p_h}}{\Delta p_h}\right]^2 + \left(\frac{\sigma_L}{L}\right)^2 + \left(2\frac{\sigma_{\dot{m}_t}}{\dot{m}_t}\right)^2 + \left(\frac{\sigma_N}{N}\right)^2} \tag{19}$$

The Reynolds number, defined by Eq. (16), is rewritten as follows,

$$\mathrm{Re} = \frac{2\dot{m}_t}{\mu N\sqrt{\pi A_f}} \tag{20}$$

The uncertainty in the Reynolds number is estimated by

$$\frac{\sigma_{\mathrm{Re}}}{\mathrm{Re}} = \sqrt{\left(\frac{\sigma_{\dot{m}_t}}{\dot{m}_t}\right)^2 + \left(\frac{\sigma_N}{N}\right)^2 + \left(\frac{\sigma_\mu}{\mu}\right)^2 + \left(\frac{1}{2}\frac{\sigma_{A_f}}{A_f}\right)^2} \tag{21}$$

The uncertainties in the cross-sectional area, number of the spirally fluted tubes, spirally fluted-tube length, density and dynamic viscosity of air due to the uncertainty in the temperature measurements are ±4.14%, 0.00%, ±0.35% for TB#1 (±0.12% for TB#2), ±0.34%, and ±0.26%, respectively.

The uncertainties in the Darcy friction factor and Reynolds number are shown in Fig. 5. As the air Reynolds number increases from 104 to 1,980, the uncertainties in the Darcy friction factor and Reynolds number of air in TB#1 decrease from 70.7% to 10.8% and 29.7% to 2.6%, respectively. Similarly, those uncertainties decrease respectively from 52.9% to 10.8% and 25.0% to 2.6% as the air Reynolds number increases from 113 to 1,818 for TB#2.

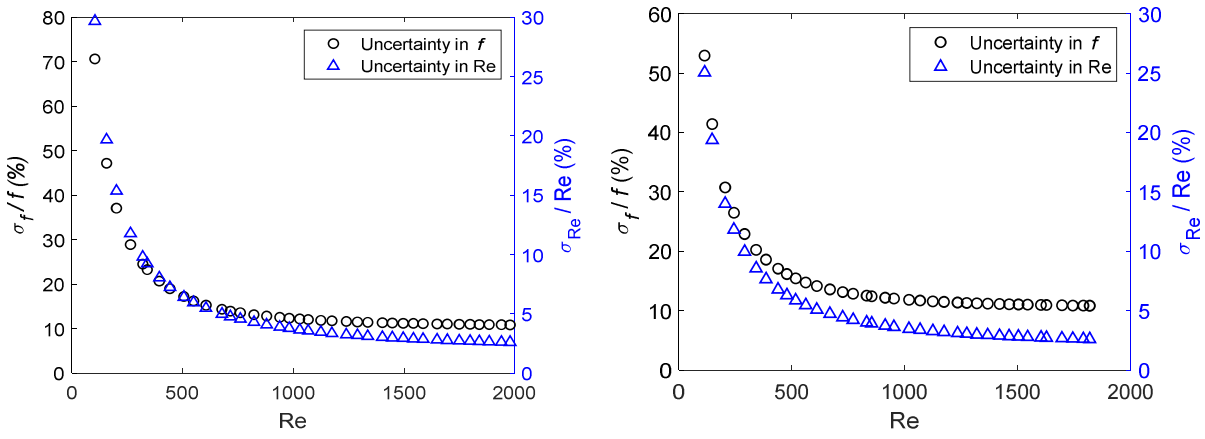

(a) (b)

Fig. 5 Uncertainties in the Darcy friction factor and Reynolds number of air in (a) TB#1 and (b) TB#2

3.1.3. Numerical model validation

As shown in Fig. 6, the Darcy friction factor for air in TB#1 is slightly larger than that in TB#2. This is because the L/D_c value is about 35.1 for the spirally fluted tube E#1 in TB#1, smaller than the L/D_c value (101.5) for E#1 in TB #2. The developing flow therefore occupies a larger fraction of E#1 in TB#1, leading to a larger Darcy friction factor. Considering their associated uncertainties, however, the two sets of experimental data are consistent with each other. In addition, it is observed that the CFD results agree reasonably well (±20% uncertainties) with the experimental data except for a few data points. Therefore, it is appropriate to apply the numerical model for the study of hydraulic performance of fluids in spirally fluted tubes.

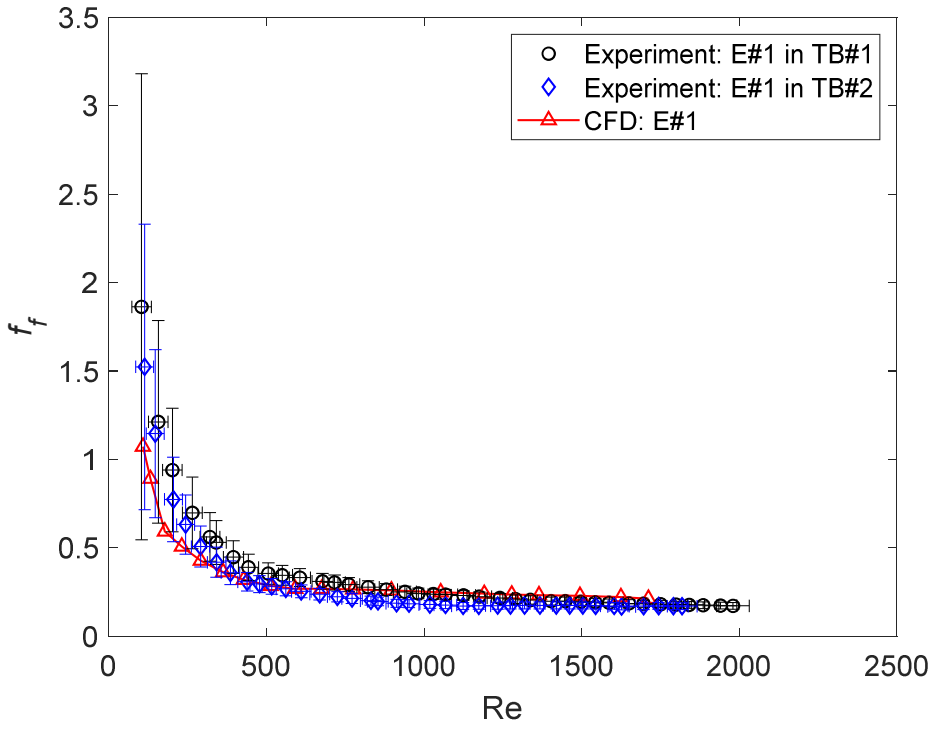

Fig. 6 Darcy friction factor for air in the spirally fluted tube E#1

3.2.Tube-side Nusselt number

The CFD results of the tube-side Nusselt number are validated by comparing with the experimental data in the literature [5]. Unlike the cross-sectional-area-averaged diameter used in this study as the characteristic length, Srinivasan [5] used the inside volumetric diameter. To have a meaningful comparison, all characteristic-length-dependent parameters in the literature [5], such as the Reynolds number and Nusselt number, are reprocessed based on the characteristic length defined in this study.

As shown in Fig. 7, the Nusselt number predicted in this study agrees well (±20% uncertainties) with the experimental data except for one abnormal data point. It is therefore appropriate to apply the numerical model for the study of thermal performance of fluids in spirally fluted tubes.

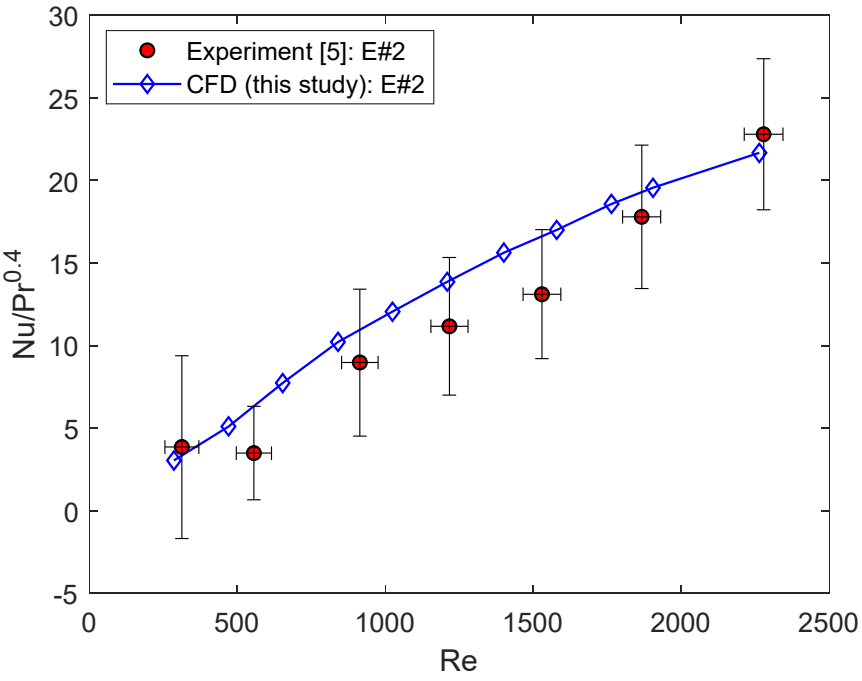

Fig. 7 Nusselt number for water in the spirally fluted tube E#2

4. Results and discussions

The effects of four geometric parameters, i.e., non-dimensional flute pitch, non-dimensional flute depth, non-dimensional flute helix angle (or flute start number), and non-dimensional trough length on convective heat transfer and friction factor characteristics of FLiNaK in spirally fluted tubes are investigated. In addition, convective heat transfer and Darcy friction factor correlations are proposed for medium-Prandtl-number fluids in spirally fluted tubes under the following conditions: Re = 88 to 1,600, Pr = 5 to 23, $p/D_c = 0.44$ to 3.51, $e/D_c =$ 0.10 to 0.40, $\theta/90 = 0.20$ to 0.81, and $L_{tr}/D_c = 0.71$ to 2.16.

4.1. Effect of the non-dimensional flute pitch

Five different values of the non-dimensional flute pitch, namely, p/D_c= 0.44, 0.94, 1.76, 2.63, and 3.51, are used for the parametric study. For any given Reynolds number (laminar flows), as shown in Fig. 8(a), the Darcy friction factor for FLiNaK in spirally fluted tubes, f_f, decreases as p/D_c increases. This is because the smaller values of p/D_c (more compact spiral flutes) normally lead to larger numbers of perturbations in a unit length experienced by the working fluid FLiNaK.

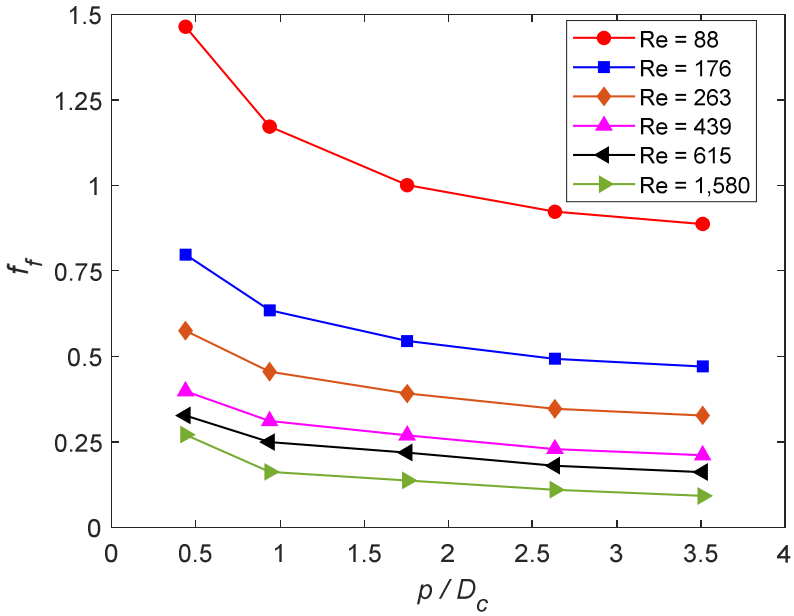

(a)

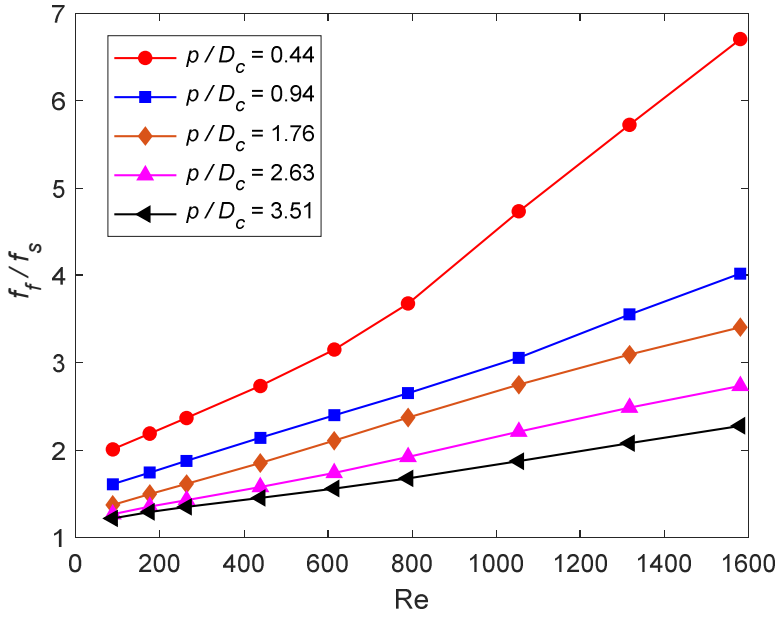

(b)

Fig. 8 Effect of the non-dimensional flute pitch on the (a) Darcy friction factor f_f and (b) friction increment ratio f_f/f_s (FLiNaK; $f_s = 64/\mathrm{Re}$; p = 5.49, 11.73, 21.94, 32.91, and 43.88 mm; e = 3.01 mm; N_s = 3; L_{tr} = 22.30 mm)

In addition, it is expected that the spirally fluted tube will eventually become a smooth tube if p/D_c is infinitely large. Taking Re = 88 as an example, as p/D_c increases from 0.44 to 3.51, f_f decreases from 1.46 to 0.89, approaching 0.73, the friction factor for fully-developed laminar flows in smooth circular tubes ($64/\mathrm{Re}$).

Compared with smooth tubes, the friction factor for fluids in spirally fluted tubes is normally much larger under the same conditions. As shown in Fig. 8(b), the friction increment ratio f_f/f_s, defined as the ratio of the Darcy friction factor between the spirally fluted tube and smooth tube, increases as the increase of the salt Reynolds number for a given p/D_c. Taking p/D_c= 0.44 as an example, f_f/f_s increases from 2.0 to 6.7 as the salt Reynolds number increases from 88 to 1,580.

As for heat transfer, the Nusselt number follows one of the two trends as p/D_c increases for a fixed Reynolds number: (1) non-monotonic decreasing and (2) monotonic decreasing.

As shown in Fig. 9(a), the Nusselt number increases initially to a peak value, then it decreases as the increase of p/D_c for small Reynolds numbers, such as Re = 105 to 1,074. This is because if p/D_c is too small (compact spiral flutes), less than a critical value, the spirally

fluted tube will act as a smooth tube and the flow may glide past the spiral flutes as observed in the experiments [5].

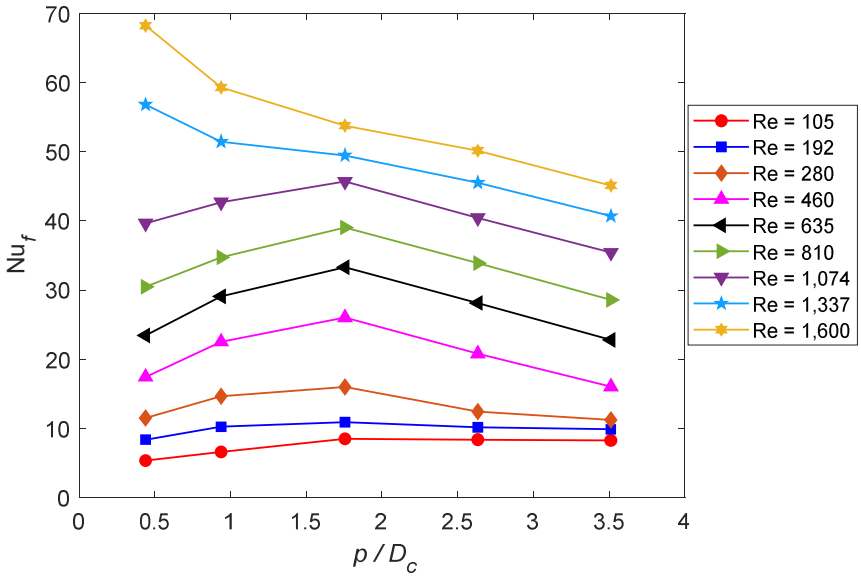

(a)

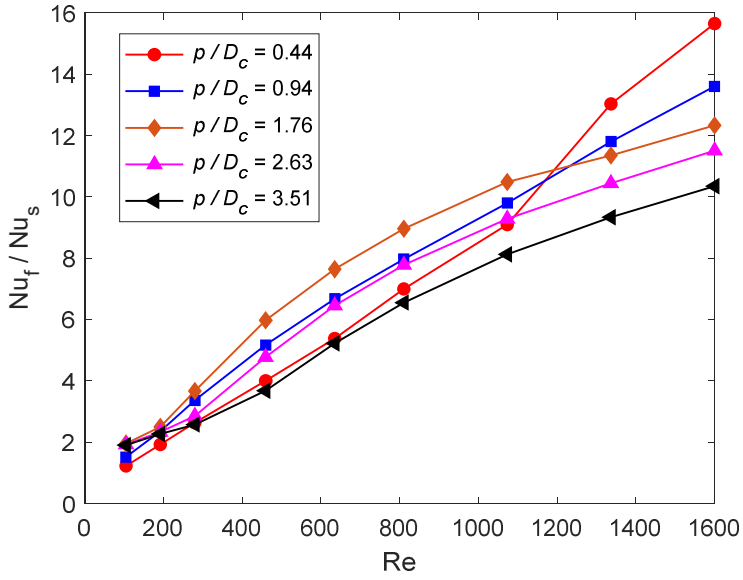

(b)

Fig. 9 Effect of the non-dimensional flute pitch on the (a) Nusselt number Nu_f and (b) heat transfer enhancement ratio Nu_f/Nu_s (FLiNaK; $Nu_s = 4.36$; p = 5.49, 11.73, 21.94, 32.91, and 43.88 mm; e = 3.01 mm; N_s = 3; L_{tr} = 22.30 mm)

For larger Reynolds numbers, Re = 1,337 to 1,600 as shown in Fig. 9(a), the Nusselt number monotonically decreases as p/D_c increases. Since the critical p/D_c value decreases as the Reynolds number increases, it is expected that the critical p/D_c value for Re = 1,337 to 1,600 is less than 0.44, which is out of the range investigated in this study.

As shown in Fig. 9(b), the heat transfer enhancement ratio, $\mathrm{Nu}_f/\mathrm{Nu}_s$, increases as the increase of the salt Reynolds number for a fixed p/D_c, where $\mathrm{Nu}_s = 4.36$ for fully-developed laminar flows in circular tubes under constant heat flux conditions. Taking p/D_c= 0.44 as an example, $\mathrm{Nu}_f/\mathrm{Nu}_s$ increases from 1.2 to 15.7 as the salt Reynolds number increases from 105 to 1,600.

4.2. Effect of the non-dimensional flute depth

Five different values of the non-dimensional flute depth, namely, e/D_c= 0.10, 0.18, 0.24, 0.33, and 0.40, are used for the parametric study. As shown in Fig. 10(a), the Darcy friction factor for FLiNaK in spirally fluted tubes, f_f, increases as e/D_c increases for a fixed Reynolds number. Taking Re = 88 as an example, the Darcy friction factor increases from 0.82 (e/D_c = 0.10) to 1.80 (e/D_c = 0.40). This is because the larger values of e/D_c (deeper spiral flutes) lead to larger fractions of the working fluid that swirl in the flute region, resulting in larger pressure drops per unit length.

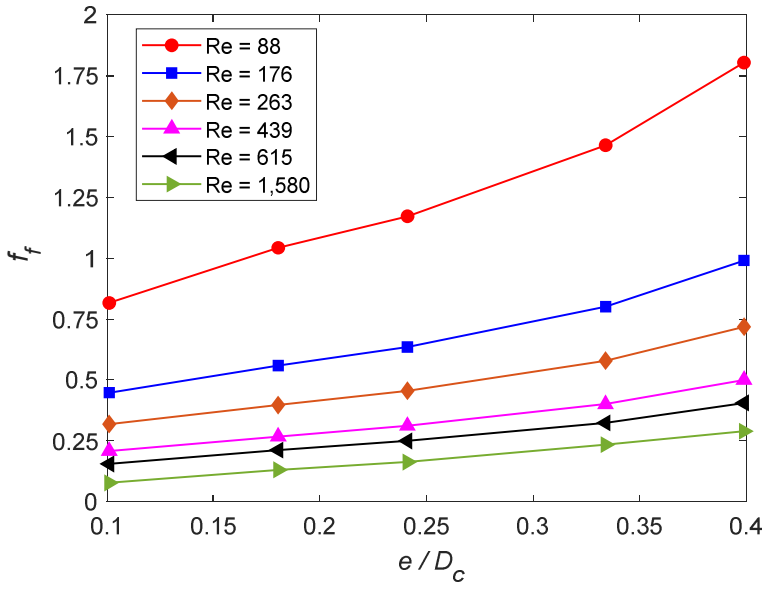

(a)

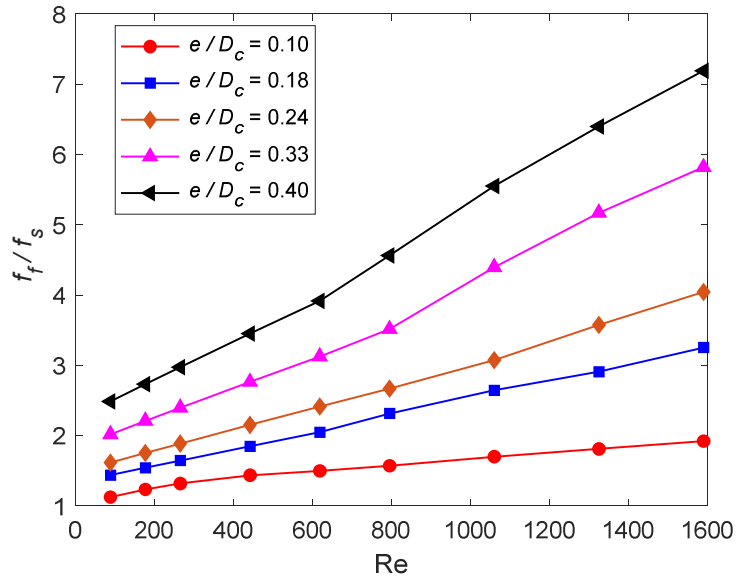

(b)

Fig. 10 Effect of the non-dimensional flute depth on the (a) Darcy friction factor f_f and (b) friction increment ratio f_f/f_s (FLiNaK; $f_s = 64/\mathrm{Re}$; p = 11.73 mm; e = 1.05, 2.19, 3.01, 4.39, and 5.49 mm; N_s = 3; L_{tr} = 22.30 mm)

The friction increment ratio f_f/f_s increases as the increase of the salt Reynolds number as shown in Fig. 10(b). Taking e/D_c= 0.40 as an example, f_f/f_s increases from 2.5 to 7.2 as the salt Reynolds number increases from 88 to 1,580.

As for heat transfer, the Nusselt number may either increase initially and decrease afterwards or monotonically decrease as e/D_c increases for a fixed Reynolds number. For large Reynolds numbers, such as Re = 280 to 1,600 as shown in Fig. 11(a), the Nusselt number increases initially to a peak value then decreases as the increase of e/D_c. This is because if e/D_c is too large (deep spiral flutes), larger than a critical value, the flow in deep spiral flutes will become stagnant, thus increasing the thermal resistance and inhibiting heat transfer between the bulk fluid and tube wall.

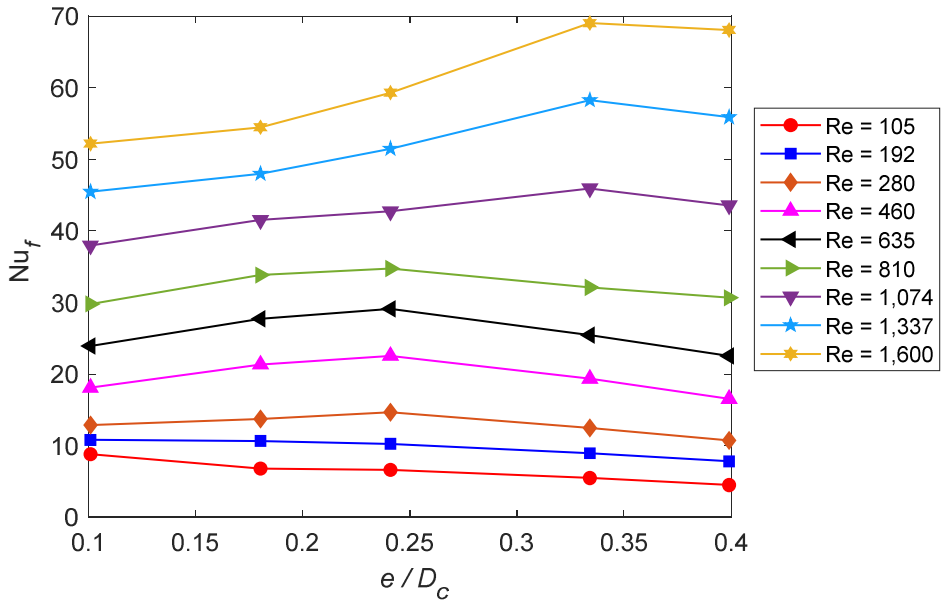

(a)

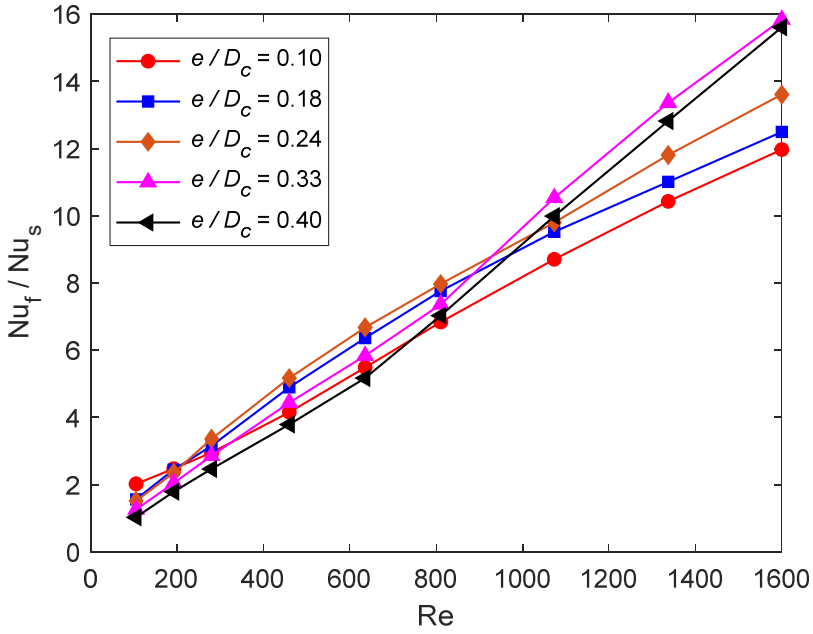

(b)

Fig. 11 Effect of the non-dimensional flute depth on the (a) Nusselt number Nu_f and (b) heat transfer enhancement ratio Nu_f/Nu_s (FLiNaK; Nu_s = 4.36; p = 11.73 mm; e = 1.05, 2.19, 3.01, 4.39, and 5.49 mm; N_s = 3; L_{tr} = 22.30 mm)

For smaller Reynolds numbers, Re = 105 to 192, a monotonic-decreasing trend is observed for the Nusselt number as shown in Fig. 11(a). In addition, the critical e/D_c value, where the Nusselt number achieves its maximum value, decreases as the Reynolds number decreases. For example, the critical e/D_c value is about 0.33 for Re = 1,600, while it decreases to 0.24 for Re = 280. Therefore, it is expected that the critical e/D_c value for Re = 105 to 192 is less than 0.10.

The heat transfer enhancement ratio Nu_f/Nu_s increases as the increase of the Reynolds number for a fixed e/D_c as shown in Fig. 11(b). For example, Nu_f/Nu_s increases from 1.3 to 15.8 as the Reynolds number increases from 105 to 1,600 for e/D_c= 0.33.

4.3. Effect of the non-dimensional flute helix angle (or flute start number)

Six different values of the flute start numbe, N_s = 1, 2, 3, 4, 5, 6 or non-dimensional flute helix angel, $\theta/90$= 0.32, 0.38, 0.46, 0.56, 0.65, and 0.81, are used for the parametric study. As

shown in Fig. 12(a), the Darcy friction factor f_f increases initially to a peak value at N_s = 4 ($\theta/90$ = 0.46), then it decreases as N_s increases or $\theta/90$ decreases. This is because there are two competing effects for larger values of N_s or smaller values of $\theta/90$: (1) stronger swirl intensity, leading to larger flow resistance and (2) narrower spiral flutes, leading to smaller flow resistance. As shown in Fig. 12(a), the former effect dominates the flow resistance for $N_s \leq 4$ ($\theta/90 \geq 0.46$), leading to an increase of the Darcy friction factor as N_s increases or $\theta/90$ decreases, while the latter effect becomes dominant for $N_s \geq 4$ ($\theta/90 \leq 0.46$), leading to a decrease of the Darcy friction factor.

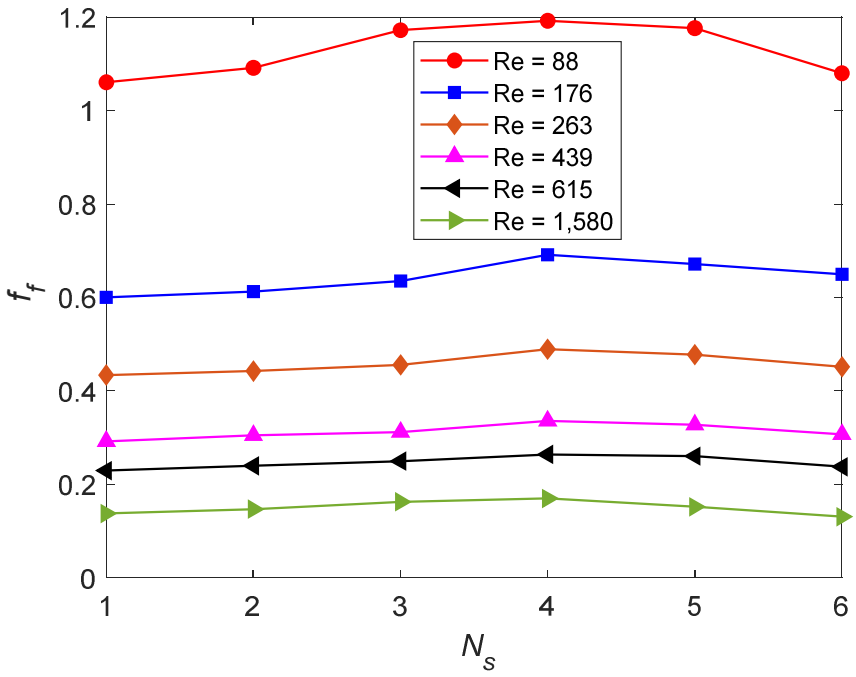

(a)

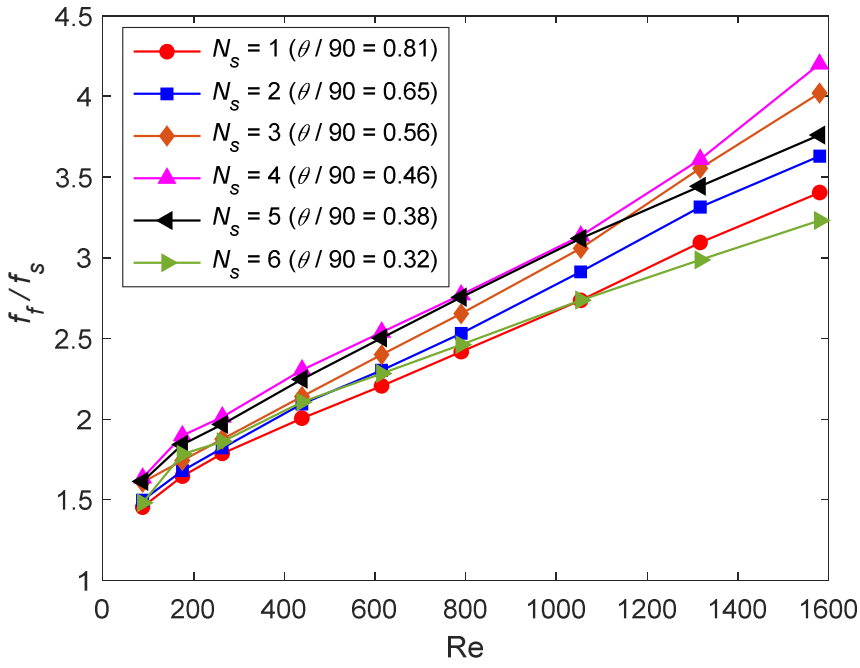

(b)

Fig. 12 Effect of the flute start number or non-dimensional flute helix angle on the (a) Darcy friction factor f_f and (b) friction increment ratio f_f/f_s (FLiNaK; $f_s = 64/\mathrm{Re}$; p = 11.73 mm; e = 3.01 mm; N_s = 1, 2, 3, 4, 5, and 6; L_{tr} = 22.30 mm)

As shown in Fig. 12(b), the friction increment ratio increases as the Reynolds number increases for a fixed N_s or $\theta/90$. For example, f_f/f_s increases from 1.64 to 4.20 for N_s = 4 or $\theta/90$ = 0.46 as the Reynolds number increases from 88 to 1,580.

As for heat transfer as shown in Fig. 13(a), the Nusselt number increases initially and then it decreases as N_s continuously increases. This is because two competing effects exist for larger values of N_s: (1) stronger swirl intensity, leading to larger heat transfer coefficients and (2) narrower spiral flutes, leading to smaller heat transfer coefficients because of the thicker stagnant or low-velocity layers in spiral flutes. In addition, the heat transfer enhancement ratio $\mathrm{Nu}_f/\mathrm{Nu}_s$ could be as high as 13.60, as shown in Fig. 13(b), for N_s = 3 or $\theta/90$ = 0.56 and Re = 1,600.

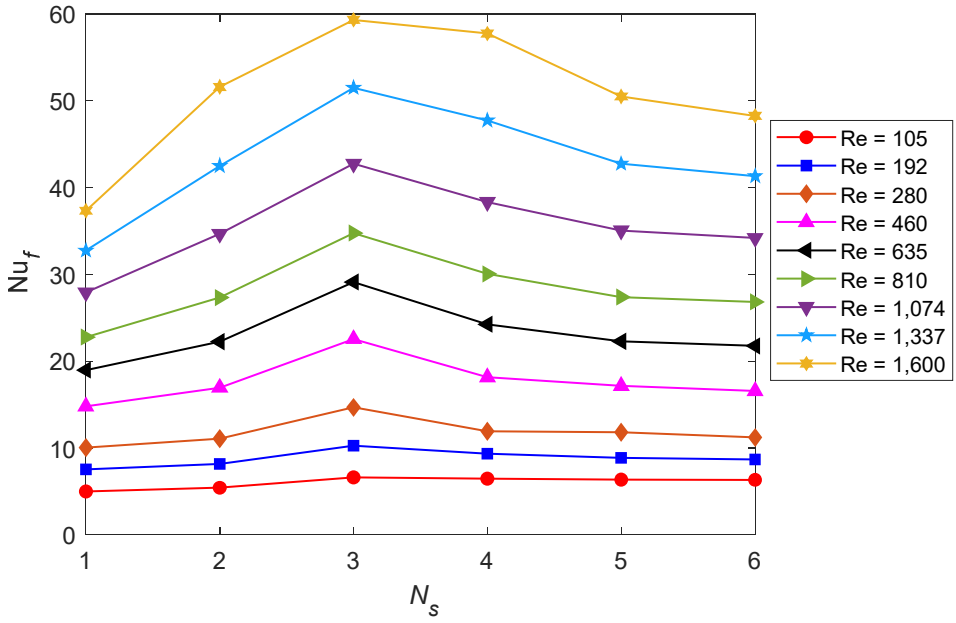

(a)

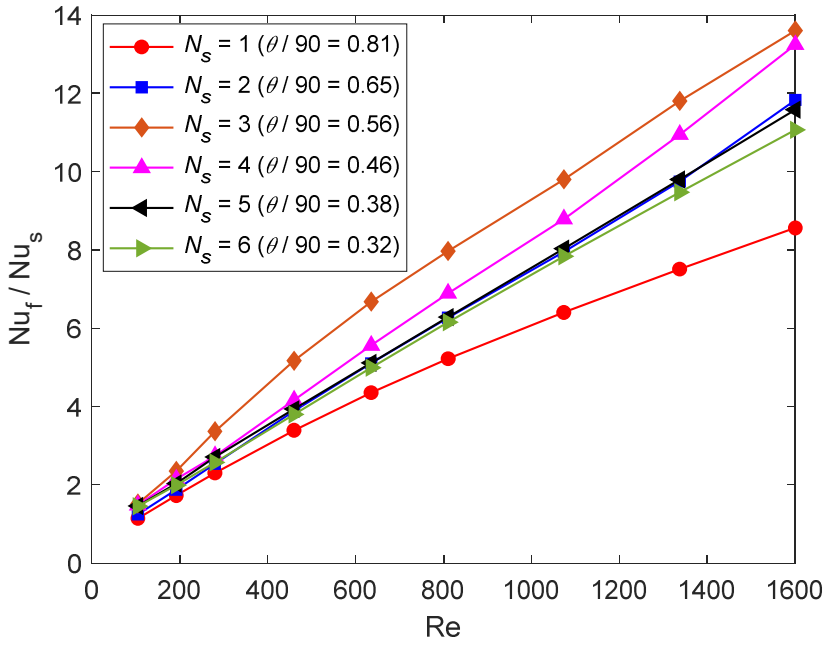

(b)

Fig. 13 Effect of the flute start number or non-dimensional flute helix angle on the (a) Nusselt number Nu_f and (b) heat transfer enhancement ratio Nu_f/Nu_s (FLiNaK; Nu_s = 4.36; p = 11.73 mm; e = 3.01 mm; N_s = 1, 2, 3, 4, 5, and 6; L_{tr} = 22.30 mm)

4.4.Effect of the non-dimensional trough length

Six different values of the non-dimensional trough length, namely, L_{tr}/D_c = 0.71, 0.97, 1.24, 1.49, 1.78, and 2.03, are used for the parametric study. As shown in Fig. 14(a), the Darcy friction factor for FLiNaK in the spirally fluted tube, f_f, decreases as the increase of the non-dimensional trough length for a fixed Reynolds number. This is because larger values of L_{tr}/D_c represent smaller fractions of the working fluid in spiral flutes, leading to smaller pressure drops per unit length.

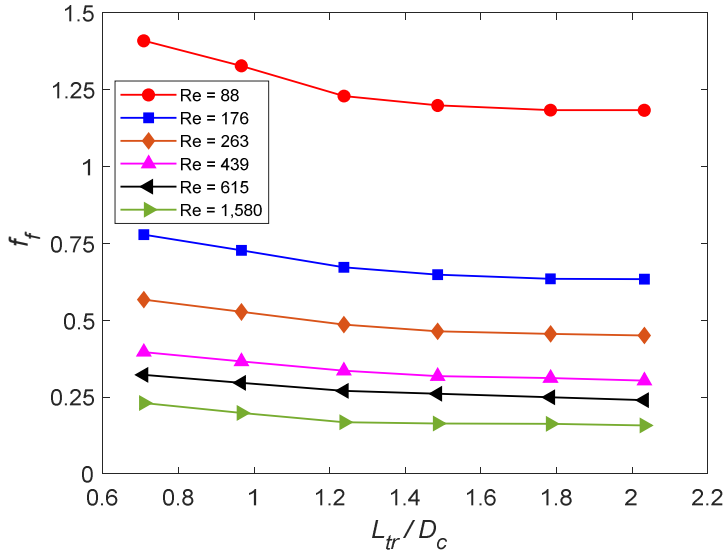

(a)

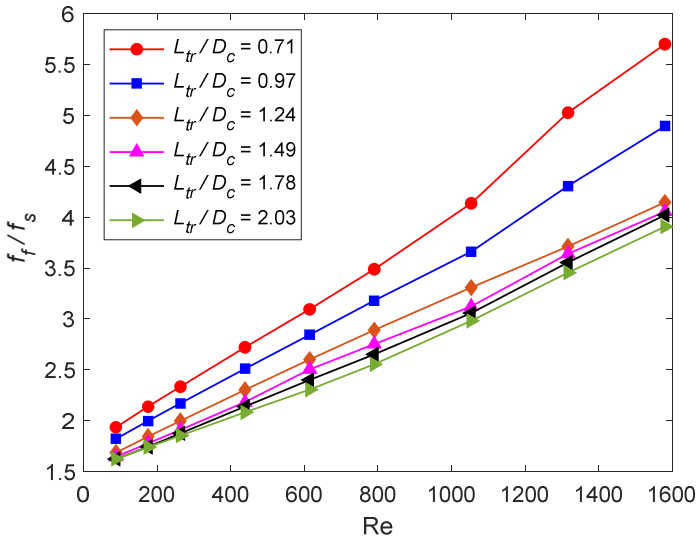

(b)

Fig. 14 Effect of the non-dimensional trough length on the (a) Darcy friction factor f_f and (b) friction increment ratio f_f/f_s (FLiNaK; $f_s = 64/\mathrm{Re}$; p = 11.73 mm; e = 3.01 mm; N_s = 3; L_{tr} = 9.52, 12.70, 15.87, 19.05, 22.30, and 25.40 mm)

In addition, the friction increment ratio f_f/f_s increases as the Reynolds number increases as shown in Fig. 14(b). For example, f_f/f_s increases from 1.94 to 5.70 as the Reynolds number increases from 88 to 1,580 for L_{tr}/D_c = 0.71.

Fig. 15(a) shows the effect of the non-dimensional trough length on the Nusselt number. The Nusselt number decreases as L_{tr}/D_c increases for a fixed Reynolds number. It is because the spirally fluted tubes with larger values of the non-dimensional trough length have narrower spiral flutes, where smaller fractions of the working fluid experience the local perturbations. In addition, the heat transfer enhancement ratio $\mathrm{Nu}_f/\mathrm{Nu}_s$ is up to 16.55 for L_{tr}/D_c = 0.71 and Re = 1,600 as shown in Fig. 15(b).

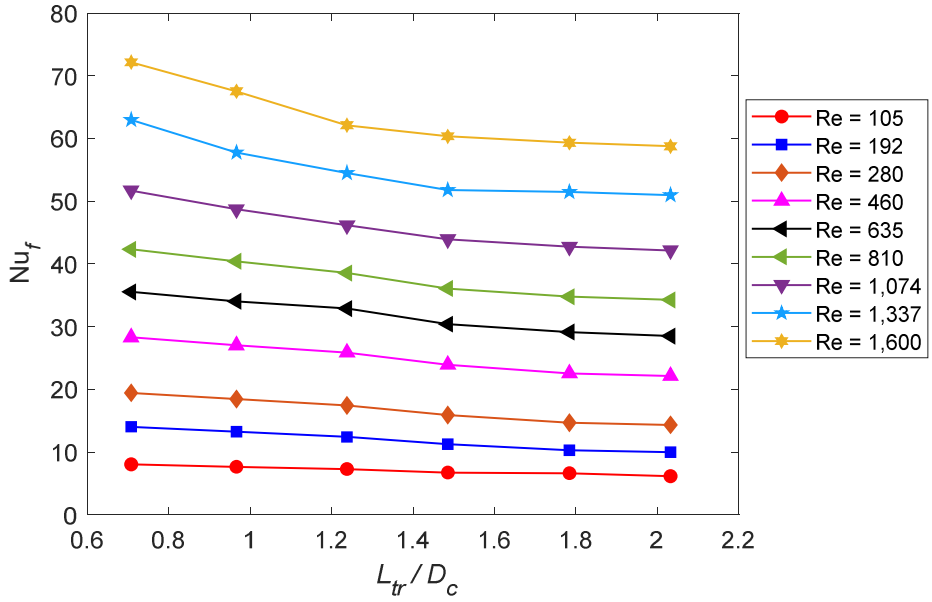

(a)

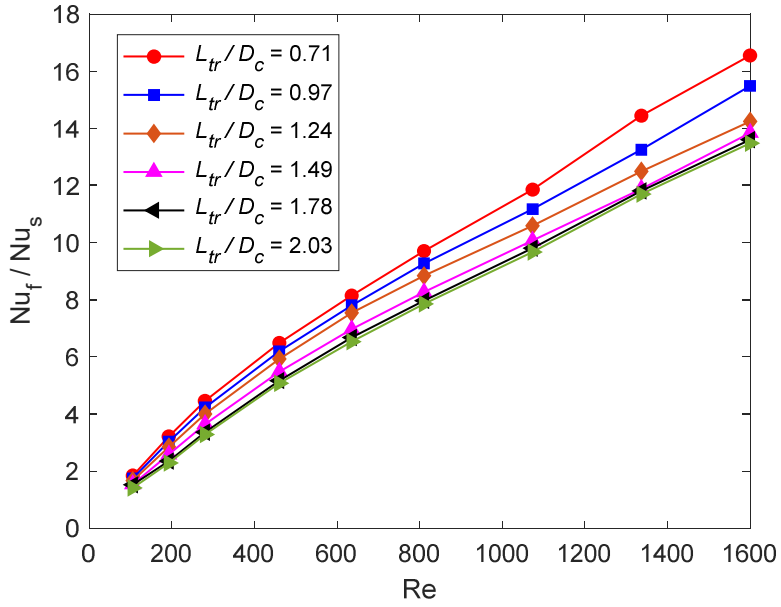

(b)

Fig. 15 Effect of the non-dimensional trough length on the (a) Nusselt number Nu_f and (b) heat transfer enhancement ratio $\mathrm{Nu}_f/\mathrm{Nu}_s$ (FLiNaK; $\mathrm{Nu}_s = 4.36$; p = 11.73 mm; e = 3.01 mm; N_s = 3; L_{tr} = 9.52, 12.70, 15.87, 19.05, 22.30, and 25.40 mm)

4.5. Friction factor correlations

The effects of the non-dimensional geometric parameters on the Darcy friction factor for spirally fluted tubes have been investigated in Sections 4.1 to 4.4 and they are also summarized as follows,

(1) As p/D_c varies from 0.44 to 3.51, the Darcy friction factor varies from 39.0% (Re = 88) to 66.7% (Re = 1,580);

(2) As e/D_c varies from 0.10 to 0.40, the Darcy friction factor varies from 54.4% (Re = 88) to 72.4% (Re = 1,580);

(3) As $\theta/90$ varies from 0.32 to 0.81, the Darcy friction factor varies from 10.9% (Re = 88) to 18.8% (Re = 1,580);

(4) As L_{tr}/D_c varies from 0.71 to 2.03, the Darcy friction factor varies from 16.3% (Re = 88) to 31.6% (Re = 1,580).

It is identified that two non-dimensional geometric parameters, p/D_c and e/D_c, have a much larger effect on the Darcy friction factor compared with the other two parameters, $\theta/90$ and L_{tr}/D_c under conditions investigated. Therefore, p/D_c and e/D_c are normally used to correlate the data in the literature as summarized in Table 1. In this study, the Darcy friction factor correlations are initially developed based on the following four different sets of the non-dimensional parameters: (1) Reynolds number, p/D_c (p^*), and e/D_c (e^*); (2) Reynolds number and e^*/p^*; (3) Reynolds number, p/D_c, e/D_c, $\theta/90$ (θ^*), and L_{tr}/D_c (L_{tr}^*); and (4) Reynolds number and $e^*/p^*L_{tr}^*\theta^*$, which are respectively expressed by

$$f = F_1(\mathrm{Re}, p^*, e^*) \tag{22a}$$

$$f = F_2\left(\mathrm{Re}, \frac{e^*}{p^*}\right) \tag{22b}$$

$$f = F_3(\mathrm{Re}, p^*, e^*, \theta^*, L_{tr}^*) \tag{22c}$$

$$f = F_4\left(\mathrm{Re}, \frac{e^*}{p^*L_{tr}^*\theta^*}\right) \tag{22d}$$

Since the power law has been widely used to correlate the friction factor data [5, 9, 13, 15], it is adopted in this study to process the data for the Darcy friction factor. Eqs. (22a) to (22d) are rewritten as

$$f = a_0\mathrm{Re}^{a_1}\left(\frac{p}{D_c}\right)^{a_2}\left(\frac{e}{D_c}\right)^{a_3} \tag{23a}$$

$$f = b_0\mathrm{Re}^{b_1}\left(\frac{e}{p}\right)^{b_2} \tag{23b}$$

$$f = c_0\mathrm{Re}^{c_1}\left(\frac{p}{D_c}\right)^{c_2}\left(\frac{e}{D_c}\right)^{c_3}\left(\frac{\theta}{90}\right)^{c_4}\left(\frac{L_{tr}}{D_c}\right)^{c_5} \tag{23c}$$

$$f = d_0\mathrm{Re}^{d_1}\left(\frac{eD_c}{pL_{tr}\theta}\right)^{d_2} \tag{23d}$$

where a_0 to a_3, b_0 to b_2, c_0 to c_5, and d_0 to d_2 are constants.

Eqs. (23a) to (23d) are linearized by applying a natural logarithm approach on both sides of these equations. A multiple linear regression approach is then adopted and performed by MATLAB for the linear forms of Eqs. (23a) to (23d) derived earlier. The Darcy friction factor correlations, developed from 171 data points of FLiNaK in nineteen spirally fluted tubes, are proposed as follows,

$$f = 53.2395\mathrm{Re}^{-0.6917}\left(\frac{p}{D_c}\right)^{-0.3714}\left(\frac{e}{D_c}\right)^{0.5704} \tag{24a}$$

$$f = 43.5191\mathrm{Re}^{-0.6917}\left(\frac{e}{p}\right)^{0.4265} \tag{24b}$$

$$f = 57.4606\mathrm{Re}^{-0.6917}\left(\frac{p}{D_c}\right)^{-0.3763}\left(\frac{e}{D_c}\right)^{0.5533}\left(\frac{\theta}{90}\right)^{-0.0514}\left(\frac{L_{tr}}{D_c}\right)^{-0.2733} \tag{24c}$$

$$f = 40.1812\mathrm{Re}^{-0.6917}\left(\frac{eD_c}{pL_{tr}\theta/90}\right)^{0.4342} \tag{24d}$$

The values of the coefficient of determination (R^2) are 0.9625, 0.9588, 0.9738, and 0.9439 for Eqs. (24a) to (24d), respectively. In addition, the residual, defined as

$$\text{Residual} = \frac{\psi_p - \psi_t}{\psi_t} \times 100\% \tag{25}$$

where ψ_p and ψ_t are respectively the predicted and true values, is plotted in Fig. 16 for each of the four correlations. It turns out that Eqs. (24a) to (24d) predict 87.7%, 85.4%, 94.7%, and 81.3% of the 171 data points within ±20% uncertainties of the true values, respectively. Therefore, it is suggested to use Eq. (24c) for predictions of the Darcy friction factor for spirally fluted tubes under the following conditions: Re = 88 to 1,580, p^* = 0.44 to 3.51, e^* = 0.10 to 0.40, θ^* = 0.20 to 0.81, and L_{tr}^* = 0.71 to 2.16.

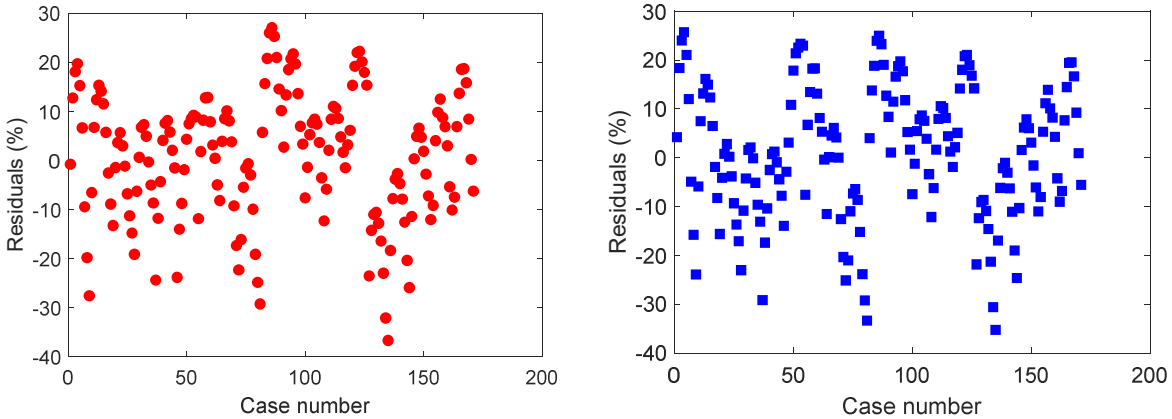

(a) (b)

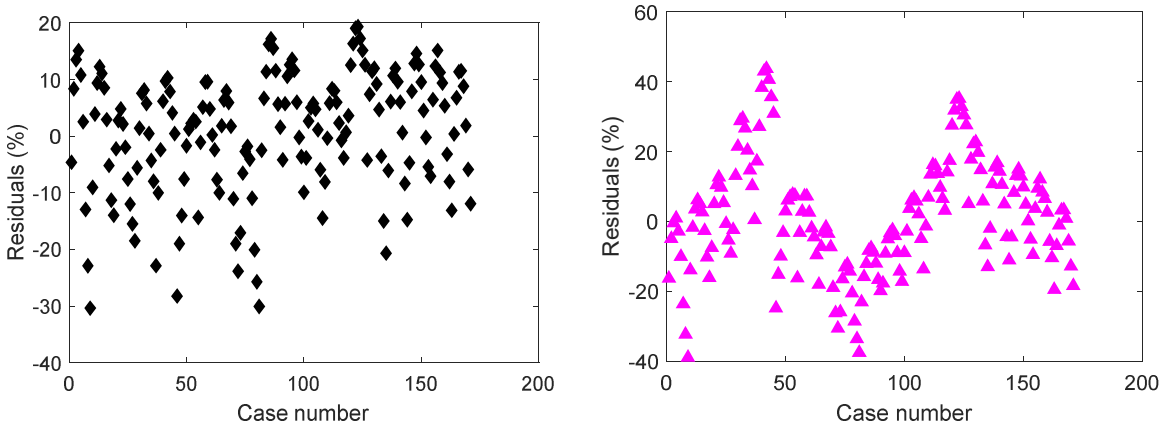

(c) (d)

Fig. 16 Residuals for different correlations used to predict the Darcy friction factor in spirally fluted tubes: (a) Eq. (24a), (b) Eq. (24b), (c) Eq. (24c), and (d) Eq. (24d)

4.6. Heat transfer correlations

The effects of the non-dimensional geometric parameters on the Nusselt number for spirally fluted tubes have been investigated in Sections 4.1 to 4.4 and they are also summarized as follows,

(1) As p/D_c varies from 0.44 to 3.51, the Nusselt number varies from 33.9% (Re = 1,600) to 37.1% (Re = 105);
(2) As e/D_c varies from 0.10 to 0.40, the Nusselt number varies from 24.3% (Re = 1,600) to 48.9% (Re = 105);
(3) As $\theta/90$ varies from 0.32 to 0.81, the Nusselt number varies from 24.8% (Re = 105) to 37.1% (Re = 1,600);
(4) As L_{tr}/D_c varies from 0.71 to 2.03, the Nusselt number varies from 18.6% (Re = 1,600) to 23.5% (Re = 105).

It is identified that variations in the Nusselt number for different values of p/D_c, e/D_c, $\theta/90$ and L_{tr}/D_c investigated are similar. Therefore, it is necessary to correlate the data with the four non-dimensional geometric parameters. As a reference, the CFD data is also correlated with p/D_c and e/D_c. In addition, it is observed that the effects of most non-dimensional geometric

parameters on the Nusselt number are not monotonous. It is therefore difficult to develop correlations similar to Eqs. (24b) and (24d) using any combined geometric parameters.

The heat transfer correlations are initially developed based on the following two different sets of the non-dimensional parameters: (1) Reynolds number, Prandtl number, p/D_c (p^*), and e/D_c (e^*) and (2) Reynolds number, Prandtl number, p/D_c, e/D_c, $\theta/90$ (θ^*), and L_{tr}/D_c (L_{tr}^*), which are respectively expressed by

$$\mathrm{Nu} = G_1(\mathrm{Re}, \mathrm{Pr}, p^*, e^*) \tag{26a}$$

$$\mathrm{Nu} = G_2(\mathrm{Re}, \mathrm{Pr}, p^*, e^*, \theta^*, L_{tr}^*) \tag{26b}$$

The power of 1/3 has been widely used for the Prandtl number of fluids in both the spirally fluted and smooth tubes [3, 15, 19]. Therefore, it is adopted for the Prandtl number in this study to correlate the data for the Nusselt number as follows,

$$\mathrm{Nu} = m_0 \mathrm{Re}^{m_1} \mathrm{Pr}^{1/3} \left(\frac{p}{D_c}\right)^{m_2} \left(\frac{e}{D_c}\right)^{m_3} \tag{27a}$$

$$\mathrm{Nu} = n_0 \mathrm{Re}^{n_1} \mathrm{Pr}^{1/3} \left(\frac{p}{D_c}\right)^{n_2} \left(\frac{e}{D_c}\right)^{n_3} \left(\frac{\theta}{90}\right)^{n_4} \left(\frac{L_{tr}}{D_c}\right)^{n_5} \tag{27b}$$

where m_0 to m_3 and n_0 to n_5 are constants.

The heat transfer correlations, developed from 171 data points of FLiNaK in nineteen spirally fluted tubes and 42 data points of water in six spirally fluted tubes, are proposed as follows,

$$\mathrm{Nu} = 0.05623 \mathrm{Re}^{0.7587} \mathrm{Pr}^{1/3} \left(\frac{p}{D_c}\right)^{-0.0274} \left(\frac{e}{D_c}\right)^{-0.1544} \tag{28a}$$

$$\mathrm{Nu} = 0.06082 \mathrm{Re}^{0.7606} \mathrm{Pr}^{1/3} \left(\frac{p}{D_c}\right)^{-0.0402} \left(\frac{e}{D_c}\right)^{-0.1649} \left(\frac{\theta}{90}\right)^{-0.0922} \left(\frac{L_{tr}}{D_c}\right)^{-0.3588} \tag{28b}$$

The values of R^2 are 0.9316 and 0.9526 for Eqs. (28a) and (28b), respectively. In addition, the residual is plotted for each of the two correlations as shown in Fig. 17. It turns out that Eqs. (28a) and (28b) predict 69.0% and 81.8% of the 213 data points within ±20% uncertainties, respectively. They also predict 85.9% and 91.5% of the data points within ±25% uncertainties, respectively. Therefore, it is suggested to use Eq. (28b) for predictions of the Nusselt number for spirally fluted tubes under the following conditions: Re = 105 to 1,600, Pr = 5 to 23, p^* = 0.44 to 3.51, e^* = 0.10 to 0.40, θ^* = 0.20 to 0.81, and L_{tr}^* = 0.71 to 2.16.

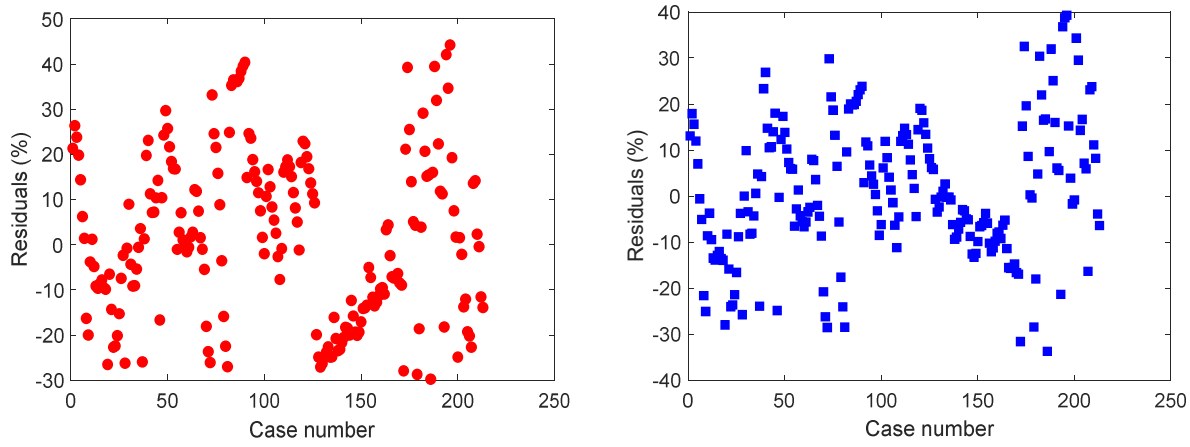

(a) (b)

Fig. 17 Residuals for different correlations used to predict the Nusselt number in spirally fluted tubes: (a) Eq. (28a) and (b) Eq. (28b)

4.7. Validation of the proposed correlations

The correlation developed for the Darcy friction factor, Eq. (24c), is validated by comparing with the experiments using (1) air as the working fluid for the spirally fluted tube E#1 in this study and (2) water as the working fluid for the spirally fluted tubes E#2 and E#3 in the literature [5].

Eq. (24c) predicts 86.7% of the total 75 data points within ±20% uncertainties as shown in Fig. 18, and 87.0% of the total 22 data points within ±20% uncertainties as shown in Fig. 19. Although the maximum relative discrepancy is as high as 52% for a few data points, the predicted values are within the experimental uncertainty. Therefore, it is appropriate to apply Eq. (24c) with ±20% uncertainties for predictions of the Darcy friction factor for spirally fluted tubes under conditions investigated.

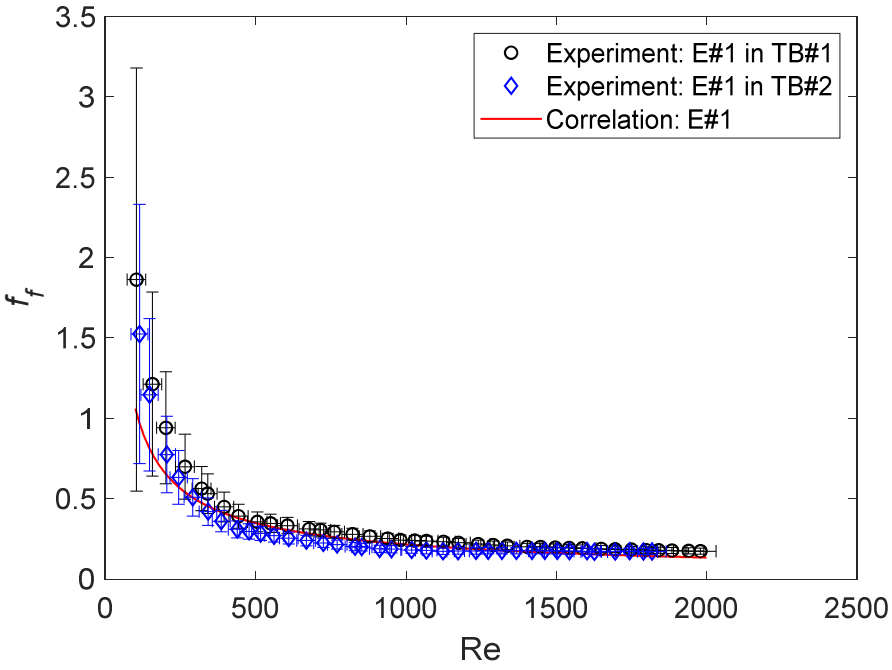

Fig. 18 Comparison of the Darcy friction factor for the spirally fluted tube E#1 between the experimental data and correlation results

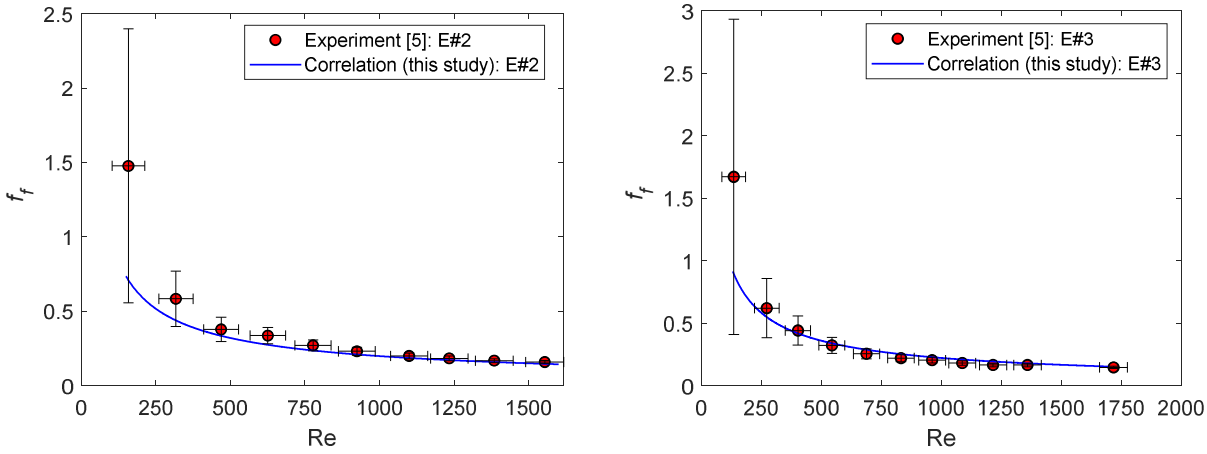

(a) (b)

Fig. 19 Comparisons of the Darcy friction factor for the spirally fluted tubes (a) E#2 and (b) E#3 between the experimental data and correlation results

The correlation developed for the Nusselt number, Eq. (28b), is validated by comparing with the experiments using (1) water (Pr = 2.5 to 7) for the spirally fluted tubes E#2 and E#3 in the

literature [5] and (2) ethylene-glycol water solution (Pr = 40) and ethylene glycol (Pr = 115) for the spirally fluted tube E#4 in the literature [3].

The relative discrepancies of the Nusselt number between the experimental data and correlation results predicted by Eq. (28b) are within ±22.4% uncertainties for E#2 except for one abnormal data as shown in Fig. 20(a) and ±7.8% uncertainties for E#3 except for one data point as shown in Fig. 20(b). In addition, the experimental data for ethylene-glycol water solution and ethylene glycol are generally within ±20% and ±30% uncertainties of the predicted values as shown in Figs. 21(a) and 21(b), respectively. The relatively large discrepancy of the Nusselt number between the experimental data and correlation results for ethylene glycol is mainly due to its large Prandlt number (Pr = 115), which is far beyond the application scope of Eq. (28b). Therefore, Eq. (28b) is applicable for Pr = 2.5 to 40 with ±20% uncertainties and Pr = 2.5 to 115 with ±30% uncertainties.

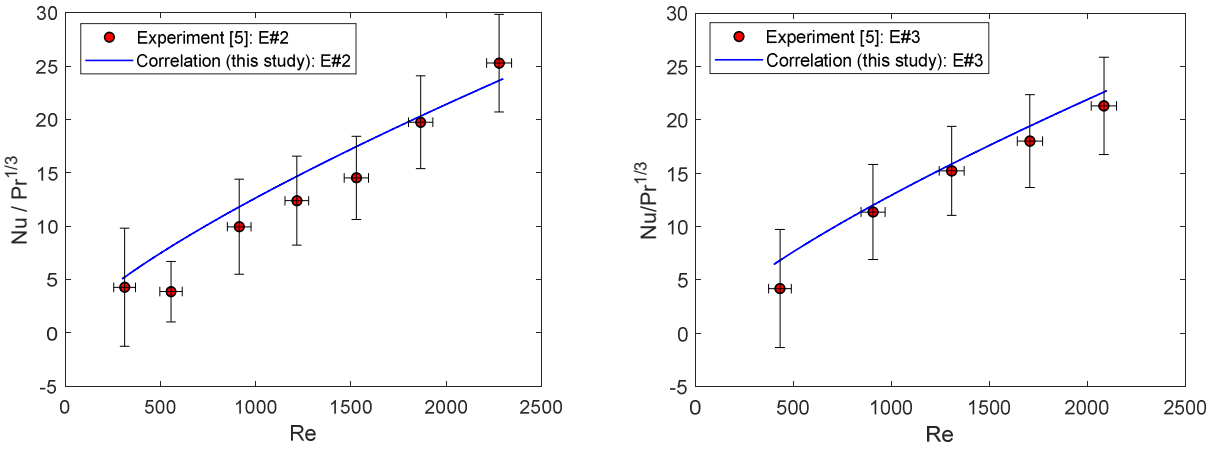

(a) (b)

Fig. 20 Comparisons of the Nusselt number for the spirally fluted tubes (a) E#2 and (b) E#3 between the experimental data and correlation results (Pr = 4.5)

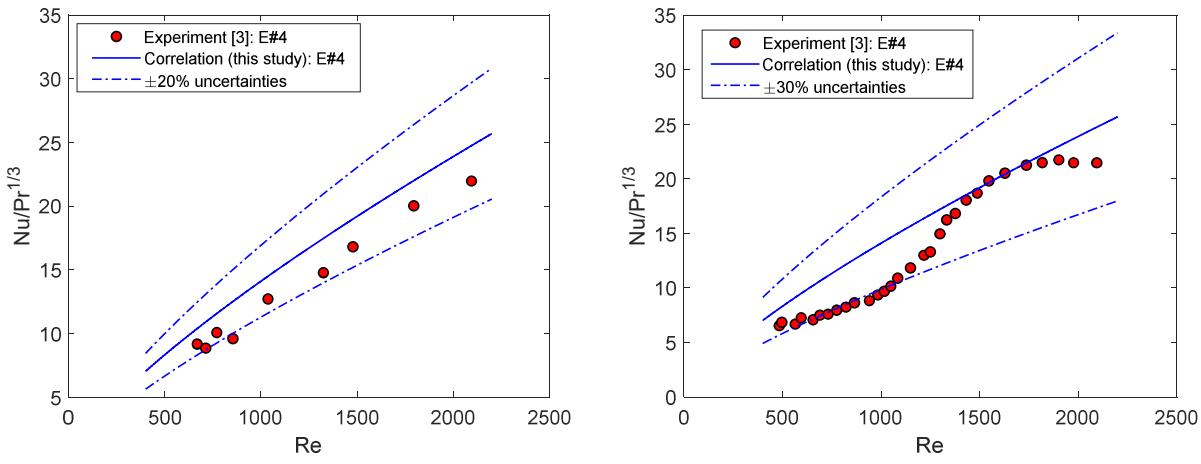

(a) (b)

Fig. 21 Comparisons of the Nusselt number for the spirally fluted tube E#4 between the experimental data and correlation results: (a) Pr = 40 and (b) Pr = 115

5. Conclusion

This study numerically investigates the effects of four non-dimensional geometric parameters, i.e., the non-dimensional flute pitch ratio ($p/D_c = 0.44$ to 3.51), non-dimensional flute depth ratio ($e/D_c = 0.10$ to 0.40), non-dimensional flute helix angle ratio ($\theta/90 = 0.20$ to 0.81), and non-dimensional trough length ratio ($L_{tr}/D_c = 0.71$ to 2.16) on thermal and hydrodynamic characteristics of FLiNaK and/or water in spirally fluted tubes using STAR CCM+. Accurate correlations for the Darcy friction factor and Nusselt number are proposed and validated for medium-Prandtl-number fluids, i.e., molten salts, in spirally fluted tubes, which help improve the design of the spirally fluted-tube HXs for molten salt applications.

Several concluding remarks are summarized as follows:

(1) The non-dimensional geometric parameters, p/D_c and e/D_c, generally have a larger effect on the Darcy friction factor and Nusselt number for spirally fluted tubes compared with the other two parameters, i.e., $\theta/90$ and L_{tr}/D_c;

(2) As the increase of p/D_c or L_{tr}/D_c, the Darcy friction factor continuously decreases. However, it increases as the increase of e/D_c. In addition, as the increase of $\theta/90$, the Darcy friction factor increases initially and then decreases under conditions investigated (Re = 88 to 1,580);

(3) As the increase of p/D_c, e/D_c, or $\theta/90$, the Nusselt number follows either a non-monotonic decreasing trend or monotonic decreasing trend, which depends on the Reynolds number. In addition, as the increase of L_{tr}/D_c, the Nusselt number continuously decreases under conditions investigated;

(4) A new Darcy friction factor correlation is suggested for spirally fluted tubes under the following conditions: Re = 88 to 1,580, p^* = 0.44 to 3.51, e^* = 0.10 to 0.40, θ^* = 0.20 to 0.81, and L_{tr}^* = 0.71 to 2.16. The associated uncertainty is about ±20% for Re = 200 to 1,580 and 36% to 52% for Re = 88 to 200.

(5) A new heat transfer correlation is suggested for spirally fluted tubes with ±20% uncertainties under the following conditions: Re = 105 to 1,600, Pr = 2.5 to 40, p^* = 0.44 to 3.51, e^* = 0.10 to 0.40, θ^* = 0.20 to 0.81, and L_{tr}^* = 0.71 to 2.16. The developed correlation is also applicable for Pr = 2.5 to 115 with ±30% uncertainties.

Conflict of interest

There is no conflict of interest.

Acknowledgment

This research was performed using funding received from the Department of Energy (DOE) Office of Nuclear Energy's Nuclear Energy University Program (NEUP). The authors appreciate the financial support from the DOE NEUP office.

References

[1] S. Zhang, H.C. Lin, K. Cheng, X. Sun, Design of a direct reactor auxiliary cooling system (DRACS) considering tritium management for Advanced High-Temperature Reactor (AHTR), Proceedings of 18th International Topical Meeting on Nuclear Reactor Thermal Hydraulics. Portland, Oregon, USA, August 18-23 (2019) 2878-2891.

[2] S. Zhang, X. Wu, S. Shi, X. Sun, R. Christensen, G. Yoder, A coupled heat transfer and tritium mass transfer model for a double-wall heat exchanger design for FHRs, Annals of Nuclear Energy 122 (2018) 328-339.

[3] S. Lee, S. Nam, T. Ban, Performance of heat transfer and pressure drop in a spirally indented tube, KSME International Journal 12 (1998) 917-925.

[4] V. Srinivasan, R. Christensen, Experimental investigation of heat transfer and pressure drop characteristics of flow through spirally fluted tubes, Experimental Thermal and Fluid Science 5 (1992) 820-827.

[5] V. Srinivasan, Experimental and numerical investigation of heat transfer and pressure drop in flow through spirally fluted tubes. PhD thesis, Ohio State University (1993).

[6] V. Srinivasan, K. Vafai, R. Christensen, Experimental investigation, modeling and prediction of frication factors and friction increase ratio for flow through spirally fluted tubes, Enhanced Heat Transfer 1 (1994) 337-350.

[7] S. Garimella, R. Christensen, Heat transfer and pressure drop characteristics of spirally fluted annuli: part I – hydrodynamics, Journal of Heat Transfer 117 (1995) 54-60.

[8] S. Garimella, R. Christensen, Heat transfer and pressure drop characteristics of spirally fluted annuli: part II – heat transfer, Journal of Heat Transfer 117 (1995) 61-68.

[9] P. Vicente, A. Garcia, A. Viedma, Experimental investigation on heat transfer and friction characteristics of spirally corrugated tubes in turbulent flow at different Prandtl numbers, International Journal of Heat and Mass Transfer 47 (2004) 671-681.

[10] Y. Qi, Y. Kawaguchi, Z. Lin, M. Ewing, R. Christensen, J. Zakin, Enhanced heat transfer of drag reducing surfactant solutions with fluted tube-in-tube heat exchanger, International Journal of Heat and Mass Transfer 44 (2001) 1495-1505.

[11] X. Chen, X. Xu, S. Nguang, A. Bergles, Characterization of the effect of corrugation angles on hydrodynamic and heat transfer performance of four-start spiral tubes, Journal of Heat Transfer 123 (2001) 1149-1158.

[12] Z. Kareem, S. Abdullah, T. Lazim, M. Jaafar, A. Wahid, Heat transfer enhancement in three-start spirally corrugated tube: experimental and numerical study, Chemical Engineering Science 134 (2015) 746-757.

[13] A. Harleß, E. Franz, M. Breuer, Experimental investigation of heat transfer and friction characteristic of fully developed gas flow in single-start and three-start corrugated tubes, International Journal of Heat and Mass Transfer 103 (2016) 538-547.

[14] J. Liu, Z. Liu, W. Liu, 3D numerical study on shell side heat transfer and flow characteristics of rod-baffle heat exchangers with spirally corrugated tubes, International Journal of Thermal Sciences 89 (2015) 34-42.

[15] Z. Jin, F. Chen, Z. Gao, X. Gao, J. Qian, Effects of pitch and corrugation depth on heat transfer characteristics in six-start spirally corrugated tube, International Journal of Heat and Mass Transfer 108 (2017) 1011-1025.

[16] H. Balla, Enhancement of heat transfer in six-start spirally corrugated tubes, Case Studies in Thermal Engineering 9 (2017) 79-89.

[17] P. Promthaisong, W. Jedsadaratanachai, V. Chuwattanakul, S. Eiamsa-ard, Heat transfer and fluid flow behaviors in a five-start spiral corrugated tube, 3rd International Conference on Chemical Materials and Process (ICMP), May 25th to 27th (2017), Beijing, China.

[18] V. Kongkaitpaiboon, P. Promthaisong, V. Chuwattanakul, K. Wongcharee, S. Eiamsa-ard, Effects of spiral start number and depth ratio of corrugated tube on flow and heat transfer characteristics in turbulent flow region, Journal of Mechanical Science and Technology 33 (2019) 4005-4012.

[19] S. Zhang, X. Sun, E.E. Dominguez-Ontiveros, Numerical study on convective heat transfer and friction characteristics of molten salts in circular tubes, Annals of Nuclear Energy 142 (2020) 107375.

[20] S. Zhang, X. Sun, Convective and radiative heat transfer in molten salts, Nuclear Technology 206 (2020) 1721-1739.

[21] L. Schwer, Is your mesh refined enough? Estimating Discretization Error using GCI, LS-DYNA Anwenderforum, Bamberg (2008).s